

# Non-Power Law Behavior in Fragmentation Cascades

Mikhail A. Belyaev<sup>1</sup> & Roman R. Rafikov<sup>1,2</sup>

## ABSTRACT

Collisions resulting in fragmentation are important in shaping the mass spectrum of minor bodies in the asteroid belt, the Kuiper belt, and debris disks. Models of fragmentation cascades typically find that in steady-state, the solution for the particle mass distribution is a power law in the mass. However, previous studies have typically assumed that the mass of the largest fragment produced in a collision with just enough energy to shatter the target and disperse half its mass to infinity is directly proportional to the target mass. We show that if this assumption is not satisfied, then the power law solution for the steady-state particle mass distribution is modified by a multiplicative factor, which is a slowly varying function of the mass. We derive analytic solutions for this correction factor and confirm our results numerically. We find that this correction factor proves important when extrapolating over many orders of magnitude in mass, such as when inferring the number of large objects in a system based on infrared observations. In the course of our work, we have also discovered an unrelated type of non-power law behavior: waves can persist in the mass distribution of objects even in the absence of upper or lower cutoffs to the mass distribution or breaks in the strength law.

*Subject headings:* Asteroids – Collisional physics – Debris disks

## 1. Introduction.

Collisional evolution of many-body astrophysical systems in which the relative velocity between colliding objects is large compared to the escape speed and coagulation is unimportant is dominated by fragmentation. Examples of such systems include the asteroid belt (Durda & Dermott, 1997; Bottke et al., 2005), the Kuiper Belt (Davis & Farinella, 1997; Pan & Sari, 2005), and debris disks around young stars (Kennedy & Wyatt, 2011; Kenyon & Bromley, 2010). As the large bodies are slowly ground down, a collisional cascade is launched, in which mass flows unidirectionally to smaller objects until at some scale it is flushed out of the system by some removal process (e.g. by Poynting-Robertson drag, radiation pressure, or gas drag).

---

<sup>1</sup>Department of Astrophysical Sciences, Princeton University, Ivy Lane, Princeton, NJ 08540; mbelyaev@astro.princeton.edu, rrr@astro.princeton.edu

<sup>2</sup>Sloan Fellow

In real astrophysical systems there is normally a large dynamic range between the scale  $m_{inj}$  at which mass is injected into the cascade and the scale  $m_{rm}$  at which mass is removed from the system. The mass  $m_{inj}$  can be defined as the mass for which the collisional destruction timescale is comparable to the age of the system. In highly evolved systems, such as the Kuiper Belt, this scale corresponds to the characteristic mass of the largest bodies (Pan & Sari, 2005; Fraser, 2009). The collision time for the smallest bodies is usually much shorter than for the largest ones, so a steady-state can be set up for  $m_{rm} \ll m \ll m_{inj}$ . In such a steady-state, the mass distribution of particles evolves on the collision timescale of bodies at the injection mass scale and can be considered static on shorter timescales.

Dohnanyi (1969) was the first to construct a model of a fragmentation cascade that aimed at explaining the mass distribution of objects in the asteroid belt. He assumed that the internal strength of colliding objects is independent of mass with the implication that  $m_B(m_t)$ , which we define as the mass of the smallest projectile capable of dispersing one half the mass of a target of mass  $m_t$  to infinity, has its mass linearly proportional to  $m_t$ . Dohnanyi also assumed that  $m_0(m_t, m_p)$ , the mass of the largest fragment produced in a collision between a target of mass  $m_t$  and a projectile of mass  $m_p$ , scales linearly with  $m_t$  and is independent of  $m_p$ . Under these assumptions, he showed that a fragmentation cascade allows a steady-state power law solution

$$n(m) \propto m^{-\alpha}, \quad \alpha = -11/6 \quad (1)$$

where  $n(m)dm$  is the number of objects in the size distribution with mass between  $m$  and  $m + dm$ .

Later, Tanaka et al. (1996) generalized Dohnanyi’s result by assuming a self-similar model of fragmentation, which again entails  $m_B(m_t) \propto m_t$ , but now  $m_0(m_t, m_p) \propto m_t q(m_p/m_t)$ , where  $q$  is an arbitrary function. They confirmed the power law form of the mass spectrum and showed that the value of  $\alpha$  is determined by the mass dependence of the collision rate and that  $\alpha$  reduces to 11/6 if the collision rate is proportional to  $m_t^{2/3}$  (geometrical cross-section with mass-independent relative velocities).

In reality, however, fragmentation does not have to be self-similar because the minimum energy necessary for disruption is not always linearly proportional to the target mass. For instance, if an object’s internal strength is dominated by gravity, then  $Q_D^*$ , the energy per unit mass required to shatter an object and disperse half of its mass to infinity, scales as  $m_t Q_D^* \propto m_t^{5/3}$ , which is the case for objects larger than  $\sim 1$  km (Benz & Asphaug, 1999; Holsapple, 1993; Benz et al, 1994). O’Brien & Greenberg (2003) considered a model in which  $Q_D^*$  scales as a power law in  $m_t$ , but took  $m_0$  linearly proportional to  $m_t$ . Under these assumptions, O’Brien & Greenberg (2003) found that a steady-state power law solution for  $n(m)$  still exists, but that  $\alpha$  differs from 11/6 unless  $Q_D^*$  is constant, even when the collision rate scales as  $m_t^{2/3}$ .

The steady-state power law solutions of Dohnanyi (1969), Tanaka et al. (1996), and O’Brien & Greenberg (2003) have since been confirmed numerous times by simulations, which have also shed light on non-power law effects present in astrophysical fragmentation cascades. These effects typically manifest themselves as waves superimposed on top of the steady-state power law solution and

are caused either by non-collisional mass sinks, e.g. due to the removal of small particles ( $\lesssim 1 \mu\text{m}$  for  $L = L_\odot$ ) by radiation pressure (Thébault & Augereau, 2007; Campo Bagatin et al., 1994; Durda & Dermott, 1997); a change in the power law index of  $Q_D^*(m_t)$  induced by a transition from the strength-dominated to the gravity-dominated regime (O’Brien & Greenberg, 2003, 2005); or a transition from a primordial to a collisionally-evolved size distribution (Fraser, 2009; Pan & Sari, 2005; Kenyon & Bromley, 2004).

In this work, we describe a new source of non-power law behavior in fragmentation cascades. We consider a model similar to the one used by O’Brien & Greenberg (2003), but with a more general form for  $m_0$ . More specifically, previous researchers (Petit & Farinella, 1993; O’Brien & Greenberg, 2005; Williams & Wetherill, 1994; Kobayashi & Tanaka, 2010; de Elía & Brunini, 2007) have typically assumed that  $m_0 = m_t p(E_{\text{coll}}/m_t Q_D^*)$ , where  $E_{\text{coll}}$  is the kinetic energy of the colliding particles in the center of mass frame, and  $p$  is a function that varies from author to author. We instead consider the more general dependence  $m_0 = m_t^\mu p(E_{\text{coll}}/m_t Q_D^*)$ , which is motivated in §2. We find that unless  $\mu = 1$ , there is no steady-state power law solution. Instead,  $n(m)$  is described by a power law with the same power law index as found by O’Brien & Greenberg (2003), but multiplied by a slowly varying function of mass (i.e.  $n(m) \propto m^{-\alpha} \varphi(m)$ ,  $|d \ln \varphi / d \ln m| \ll 1$ ). The non-power law effects caused by the slowly varying function show up as a smooth deviation from power-law behavior, which is quite different from the wave-like features described earlier. This deviation is significant when extrapolating over many orders of magnitude in mass, as demonstrated in §6.3.

In the course of our investigation, we have also discovered that it is possible for waves to appear and persist in a collisional cascade, even if the particle size distribution does not contain an upper or lower mass cutoff, and the strength is described by a pure power law with no breaks. This is a completely independent type of non-power law behavior from the one caused by  $m_0$  not proportional to  $m_t$ . In astrophysical systems, such waves may be triggered by stochastic collision events between large planetesimals (Kenyon & Bromley, 2005; Wyatt & Dent, 2002; Wyatt, 2008). However, the main focus of our paper is on the non-power law behavior that results when  $m_0$  is not proportional to  $m_t$ , and we defer a detailed discussion of these waves for the future.

The paper is organized as follows. In §2, we introduce the general equations describing fragmentation and discuss specific assumptions relevant to our model. In §3 we demonstrate that pure power law solutions for a fragmentation cascade are indeed possible if  $m_0 \propto m_t p(E_{\text{coll}}/m_t Q_D^*)$ , consistent with Kobayashi & Tanaka (2010). We show in §4 that if the assumption  $m_0 \propto m_t$  is not satisfied, then solutions are given by the product of a power law with the same index as in the  $m_0 \propto m_t$  case, and a slowly varying function of mass. We then find analytic solutions for this slowly varying function for monodisperse (all fragments having the same mass) and power law fragment mass distributions. We find that in the monodisperse case, the solutions for the steady-state distribution are not unique and can support waves. We confirm our analytical results numerically in §5 and discuss their validity and possible applications in §6.

## 2. Basic setup

The number density distribution of particles in mass space,  $n(m)$ , obeys the continuity equation (Tanaka et al., 1996):

$$\frac{\partial n(m)m}{\partial t} + \frac{\partial F(m)}{\partial m} = 0, \quad (2)$$

where the mass flux,  $F(m)$  is defined to be the amount of mass which flows past a point  $m$  in mass space per unit time. We will consider the evolution of the mass spectrum for  $m \ll m_{inj}$  in which case we can adopt the steady-state assumption. Under this assumption,  $F(m)$  is constant, so there is no accumulation of particles at any scale.

In order to write down the explicit form of  $F(m)$ , we need to make some definitions. Disruption of a target in a collision produces a spectrum of fragments characterized by the function  $g(m_f, m_t, m_p)$ , where  $g(m_f, m_t, m_p)dm_f$  is the number of fragments in the mass interval  $(m_f, m_f + dm_f)$  coming *only from the target* in a collision between bodies with mass  $m_p$  and  $m_t$ . Mass conservation then requires that

$$\int_0^\infty g(m_f, m_t, m_p)m_f dm_f = m_t. \quad (3)$$

Kobayashi & Tanaka (2010) have shown that erosive collisions provide the dominant contribution to the mass flux, and in order to take them into account, it is useful to split  $g$  into two components

$$g(m_f, m_t, m_p) = g_{rem}(m_f, m_t, m_p) + g_{ej}(m_f, m_t, m_p). \quad (4)$$

Here,  $g_{ej}$  is the contribution to the mass flux from the continuous distribution of fragments ejected from the target and is normalized such that

$$\int_0^\infty g_{ej}(m_f, m_t, m_p)m_f dm_f = m_{ej}(m_t, m_p), \quad (5)$$

where  $m_{ej}$  is the total amount of mass ejected from the target and dispersed to infinity. In catastrophic collisions with  $m_p \gg m_B$ ,  $m_{ej} = m_t$ . However, in collisions with  $m_p \lesssim m_B$ , the core of the target is left almost intact (Fujiwara et al., 1977), leaving behind a remnant of mass  $m_{rem} = m_t - m_{ej}$ . This yields

$$g_{rem}(m_f, m_t, m_p) = \delta(m_f - m_{rem}(m_t, m_p)). \quad (6)$$

When  $m_p = m_B$ , then by definition of  $m_B$ ,  $m_{rem} = m_{ej} = m_t/2$ . A collision is commonly referred to as catastrophic when  $m_{ej} > m_{rem}$  and as erosive when  $m_{ej} < m_{rem}$ . We also clarify that  $m_0$  is the largest fragment in the continuous distribution of ejecta,  $g_{ej}$ , to which  $m_{rem}$  does *not* belong.

We next define  $f(m, m_t, m_p)$  as the mass fraction of debris with  $m_f < m$ , which comes from the target only in a collision between a target of mass  $m_t$  and a projectile of mass  $m_p$ :

$$f(m, m_t, m_p) = \frac{1}{m_t} \int_0^m g(m_f, m_t, m_p) m_f dm_f. \quad (7)$$

This is consistent with Tanaka et al. (1996) and Kobayashi & Tanaka (2010) and allows for projectiles that are larger than targets. We next split  $f$  into two parts, just as we did with  $g$ :

$$f(m, m_t, m_p) = f_{ej}(m, m_t, m_p) + f_{rem}(m, m_t, m_p). \quad (8)$$

Using the definitions (5), (6), and (7), we have

$$f_{ej}(m, m_t, m_p) = \frac{1}{m_t} \int_0^m g_{ej}(m_f, m_t, m_p) m_f dm_f, \quad (9)$$

and

$$f_{rem}(m, m_t, m_p) = \begin{cases} m_{rem}(m_t, m_p)/m_t & , \quad m > m_{rem}(m_t, m_p) \\ 0 & , \quad m < m_{rem}(m_t, m_p) \end{cases}. \quad (10)$$

We can now write down the mass flux in the form

$$F(m) = - \int_m^\infty dm_t m_t n(m_t) \int_0^\infty dm_p f(m, m_t, m_p) n(m_p) \mathcal{R}(m_t, m_p), \quad (11)$$

where  $\mathcal{R}(m_t, m_p)$  is the collision rate between bodies with mass  $m_t$  and  $m_p$ . The utility of splitting  $f$  into two components (Eq. 8) will become apparent shortly in §2.2.

## 2.1. Some simplifications

When gravitational focusing is unimportant, the collision rate is given by

$$\mathcal{R}(m_t, m_p) = \pi \left( \frac{3}{4\pi\rho} \right)^{2/3} \left( m_t^{1/3} + m_p^{1/3} \right)^2 \langle v \rangle^2, \quad (12)$$

where  $\langle v \rangle$  is an averaged collision velocity, which can be a function of  $m_t$  and  $m_p$ . To limit the number of parameters in our study, we will assume

$$\langle v \rangle = \text{const}, \quad (13)$$

so the collision rate becomes

$$\mathcal{R}(m_t, m_p) \propto \left( m_t^{1/3} + m_p^{1/3} \right)^2, \quad (14)$$

but our results are easily extended to the forms of  $\mathcal{R}$  considered by Tanaka et al. (1996), who varied the power law dependence of  $\mathcal{R}$  on  $m_t$  and  $m_p$ .

It is natural to expect that disruption of targets with mass  $m_t$  is dominated by collisions with projectiles having masses near or below the breaking threshold  $m_B(m_t)$ . This is because the cross-section for catastrophic collisions (defined by  $m_p > m_B(m_t)$  (§2)) is dominated by the smallest particles as long as  $\alpha > 5/3$  (Dohnanyi, 1969), and the mass flux from erosive collisions drops off for  $m_p \ll m_B(m_t)$  (Kobayashi & Tanaka, 2010). We now assume

$$m_B(m_t) \ll m_t, \quad (15)$$

which is typically valid for astrophysical fragmentation cascades. Then,  $\mathcal{R}(m_t) \propto m_t^{2/3}$  for collisions that are responsible for the majority of the mass flux. This allows us to rewrite (11) in the following form:

$$F(m) \propto \int_m^\infty dm_t m_t n(m_t) \mathcal{R}(m_t) \int_0^\infty dm_p f(m, m_t, m_p) n(m_p). \quad (16)$$

The normalization of  $F(m)$  is unimportant since the only thing that matters for a steady-state solution is that  $F(m)$  is constant.

## 2.2. Fragmentation Model

Experimental data on collisional breakup (Gault & Wedekind, 1969; Fujiwara et al., 1977) and numerical simulations of high-velocity collisions (Benz et al, 1994; Benz & Asphaug, 1999) suggest that the mass spectrum of fragments ejected from the target in a single collision can be reasonably well fit within a broad range of masses by a power-law with a cutoff at  $m_0(m_t, m_p)$ <sup>1</sup>:

$$g_{ej}(m_f, m_t, m_p) \propto \begin{cases} m_f^{-\eta(m_t, m_p)} & , \quad m_f < m_0(m_t, m_p) \\ 0 & , \quad m_f > m_0(m_t, m_p) \end{cases} \quad (17)$$

Equation (17) is difficult to analyze for arbitrary dependencies of  $\eta(m_t, m_p)$  and  $m_0(m_t, m_p)$ . Thus, we make the simplification, motivated in §2.3 that  $g_{ej}(m_f, m_t, m_p)$  has the form<sup>2</sup>

$$g_{ej}(m_f, m_t, m_p) = \frac{m_{ej}(m_t, m_p)}{m_{0,B}^2(m_t)} \psi \left( \frac{m_f}{m_{0,B}(m_t)}, \frac{E_{coll}(m_t, m_p)}{m_t Q_D^*(m_t)} \right), \quad m_{0,B}(m_t) \equiv m_0(m_t, m_B(m_t)). \quad (18)$$

In the limit  $m_p \ll m_t$ ,

$$E_{coll}(m_t, m_p) \approx m_p \langle v \rangle^2 / 2, \quad (19)$$

---

<sup>1</sup>Fujiwara et al. (1977), Takagi et al. (1984), Davis & Ryan (1990) find that a two or three slope power law better fits the data.

<sup>2</sup>In some sense, this is more general than the form (17), because  $g_{ej}$  does not have to be a power law.

which together with the assumptions (15) and the definition<sup>3</sup>

$$E_{coll}(m_t, m_B(m_t)) = Q_D^*(m_t)m_t \quad (20)$$

implies

$$\frac{E_{coll}(m_t, m_p)}{m_t Q_D^*(m_t)} = \frac{m_p}{m_B(m_t)}, \quad m_B(m_t) \ll m_t. \quad (21)$$

It now helps to define the variables

$$x \equiv m/m_{0,B}(m_t) \quad (22)$$

$$y \equiv m_p/m_B(m_t) \quad (23)$$

$$z \equiv m/m_t \quad (24)$$

Then, with the form of  $g_{ej}$  given by Eq. (18),  $f_{ej}$  becomes

$$f_{ej}(m, m_t, m_p) = \frac{m_{ej}(m_t, m_p)}{m_t} \xi(x, y). \quad (25)$$

The normalization of  $\xi$  is such that  $\xi(\infty, y) = 1$ , for  $y > 0$ , which follows from Eq. (5) and Eq. (9).

The prefactor in Eq. (25) can be written as

$$\frac{m_{ej}(m_t, m_p)}{m_t} = 1 - \frac{m_{rem}(m_t, m_p)}{m_t}. \quad (26)$$

If we now make the assumption that

$$\frac{m_{rem}(m_t, m_p)}{m_t} = \chi(y), \quad (27)$$

we can absorb the prefactor in Eq. (25) and write

$$f_{ej}(m, m_t, m_p) = f_{ej}(x, y). \quad (28)$$

One can consider more general prescriptions for  $m_{rem}/m_t$  than Eq. (27), but the latter suffices to illustrate the non-power law behavior. It also follows from Eq. (27) that  $f_{rem}$  has the form

$$f_{rem}(z, y) = \begin{cases} \chi(y) & , \quad z > \chi(y) \\ 0 & , \quad z < \chi(y) \end{cases}, \quad (29)$$

so that finally we arrive at

$$f(m, m_t, m_p) = f_{rem}(z, y) + f_{ej}(x, y). \quad (30)$$

---

<sup>3</sup>Some authors (e.g. O'Brien & Greenberg (2005)) assume that the projectile absorbs half of the energy, so  $E_{coll}(m_t, m_B(m_t)) = 2Q_D^*m_t$ , but it does not matter which definition is adopted for our purposes.

### 2.3. Nonlinear scaling of $m_{0,B}(m_t)$ .

We now address the natural question of whether one should expect a nonlinear scaling of  $m_{0,B}(m_t)$  in practice? Experimental (Fujiwara et al., 1977) and numerical (Benz & Asphaug, 1999) studies of collisional fragmentation suggest that the mass of the largest fragment formed in a high-speed catastrophic collision decreases with increasing collision energy. In particular, we focus on the experiments of Fujiwara et al. (1977), who fired polycarbonate projectiles of a constant mass and kinetic energy ( $m_p = .37$  g  $v_p = 2.6$  km s<sup>-1</sup>) into basalt targets with masses in the range  $22$  g  $< m_t < 2900$  g. They fit their data in the catastrophic regime with the following relation:

$$\max[m_0(m_t|m_p, v_p), m_{rem}(m_t|m_p, v_p)] \propto m_t \left( \frac{E_{coll}(m_t|m_p, v_p)}{m_t} \right)^{-\gamma}, \quad \gamma \approx 1.24. \quad (31)$$

The vertical bar denotes the fact that the experiments of Fujiwara et al. (1977) were performed at constant projectile mass and velocity. Since  $E_{coll}(m_t|m_p, v_p) \approx \text{const}$  for  $m_p \ll m_t$ , what Fujiwara et al. (1977) have shown is that  $m_0(m_t|m_p, v_p) \propto m_t^{1+\gamma}$ . However, we now make the following extension to their results. We assume Eq. (31) to be valid as a function of  $m_p$  as well, so we write

$$\max[m_0(m_t, m_p|v_p), m_{rem}(m_t, m_p|v_p)] \propto m_t \left( \frac{E_{coll}(m_t, m_p|v_p)}{m_t} \right)^{-\gamma} \quad (32)$$

In the highly catastrophic fragmentation regime ( $E_{coll} \gg m_t Q_D^*$ ), we expect all of the fragments to be a part of the continuous fragment distribution, so that there is no remnant mass remaining ( $m_{rem} = 0$ ). This means we can simplify Eq. (32) to the form

$$m_0(m_t, m_p|v_p) \propto m_t \left( \frac{E_{coll}(m_t, m_p|v_p)}{m_t} \right)^{-\gamma}. \quad (33)$$

Using  $m_p = m_B(m_t)$  in Eq. (19) and making the usual assumption (13) then yields

$$\frac{m_{0,B}(m_t)}{m_t} \propto \left( \frac{m_B(m_t)}{m_t} \right)^{-\gamma}. \quad (34)$$

Thus, unless  $m_B \propto m_t$ ,  $m_{0,B}$  is *not* proportional to  $m_t$ . Moreover, we see that if  $m_B$  varies as a power law, then  $m_{0,B}$  varies as a power law as well. One assumption that we have made in deriving Eq. (34) is that Eq. (33) is valid for  $m_0 \lesssim m_t$ , even though Fujiwara et al. (1977) obtained the power law relationship (Eq. (31)) by fitting primarily to data in the regime  $m_0 \ll m_t$ . Nevertheless, our analysis has shown that a power law dependence for  $m_{0,B}$  is plausible, and we discuss the matter further in §6.2.

We now deduce what we would expect for the power law exponent of  $m_{0,B}(m_t)$  in the range of target masses considered by Fujiwara et al. (1977). Experiments and simulations (Benz & Asphaug, 1999; Holsapple, 1993; Housen et al., 1991; Benz et al, 1994) show that  $Q_D^*$  is well-described over a large range of masses by the expression

$$Q_D^*(m_t) = Q_0 m_t^{s/3}, \quad (35)$$



where the exponent  $s$  is different for the strength-dominated and gravity-dominated regimes. If  $\langle v \rangle$  is constant as we have been assuming, then it follows from Eq. (21) that

$$m_B(m_t) = Bm_t^\beta, \quad \beta = 1 + s/3, \quad (36)$$

and consequently

$$m_{0,B}(m_t) = Cm_t^\mu, \quad \mu = 1 - \gamma s/3. \quad (37)$$

From simulations of impacts into basalt with  $v_p = 3 \text{ km s}^{-1}$ , Benz & Asphaug (1999) found that  $s = -.38$  in the strength-dominated regime. Using  $\gamma = 1.24$ , the value measured by Fujiwara et al. (1977) yields  $\mu = 1.16$ . This is a small deviation from  $m_{0,B} \propto m_t$  (i.e.  $\mu = 1$ ), but enough to cause noticeable effects for real systems as we demonstrate in §6.3.

We next motivate our form for  $g_{ej}$  in §2.2 by assuming the more general form

$$g_{ej}(m_f, m_t, m_p) = \frac{m_{ej}(m_t, m_p)}{m_0^2(m_t, m_p)} \psi_1 \left( \frac{m_f}{m_0(m_t, m_p)}, y \right) \quad (38)$$

and showing that it reduces to Eq. (18) if  $m_0(m_t, m_p)$  is given by Eq. (33) (with the assumption  $v_p = \text{const}$ ). Using Eq. (19) and Eq. (34) in Eq. (33), we can write

$$m_0(m_t, m_p) \propto m_{0,B}(m_t) \left( \frac{m_p}{m_B(m_t)} \right)^{-\gamma}. \quad (39)$$

Substituting this expression into Eq. (38) and using the definition of  $y$  from Eq. (23), yields

$$g_{ej}(m_f, m_t, m_p) = \frac{m_{ej}(m_t, m_p)}{(m_{0,B}(m_t)y^{-\gamma})^2} \psi_1 \left( \frac{m_f}{m_{0,B}(m_t)} y^\gamma, y \right). \quad (40)$$

Making the definition  $\psi(x, y) = y^{2\gamma} \psi_1(xy^\gamma, y)$ , we arrive at Eq. (18).

### 3. Power Law Solutions

We now look for a steady-state power law solution for the mass distribution. Plugging Eq. (1) into Eq. (16), using  $\mathcal{R}(m_t) \propto m_t^{2/3}$ , and using the form of  $f$  given in Eq. (30) yields

$$F(m) \propto \int_m^\infty dm_t m_t^{5/3-\alpha} \int_0^\infty dm_p m_p^{-\alpha} (f_{rem}(z, y) + f_{ej}(x, y)). \quad (41)$$

We now demonstrate how the power law solutions previously derived in the literature follow from this equation and elucidate under what conditions they fail.

### 3.1. Dohnanyi (1969) and Tanaka et al. (1996) case

Dohnanyi (1969) and Tanaka et al. (1996) assumed a scale-free model of fragmentation with  $f(m, m_t, m_p) = f(m/m_t, m_p/m_t)$ , which in Dohnanyi’s case was stated simply as  $m_0 = Cm_t$  with  $C$  constant, and  $m_B = Bm_t$  with  $B$  constant. From Eq. (30), we see that this is equivalent to assuming  $m_{0,B} \propto m_t$  and  $Q_D^*$  is constant. Changing the variables of integration to  $x = z = m/m_t$  and  $y = m_p/m_t$  in Eq. (41), and using Eq. (8) we have

$$F(m) \propto m^{11/3-2\alpha} \int_0^1 dx x^{2\alpha-14/3} \int_0^\infty dy y^{-\alpha} f(x, y). \quad (42)$$

Taking  $\alpha = 11/6$  results in  $F(m)$  being constant in agreement with Dohnanyi (1969) and Tanaka et al. (1996), and we discuss the conditions under which the integrals in Eq. (42) converge in Appendix A. We will subsequently call a fragmentation model with  $m_{0,B} = Cm_t$  and  $m_B = Bm_t$  a “Dohnanyi model”.

### 3.2. O’Brien & Greenberg (2003) and Kobayashi & Tanaka (2010) case

O’Brien & Greenberg (2003) and Kobayashi & Tanaka (2010) went one step further and considered a power law dependence of the strength as given by Eq. (35). If  $s = 0$  in Eq. (35) (i.e.  $\beta = 1$  in Eq. (36)), then this reduces to the Dohnanyi model. At the same time, O’Brien & Greenberg (2003) and Kobayashi & Tanaka (2010) still took  $m_{0,B} = Cm_t$ , so in their case  $x = z = m/m_t$  and  $y = m_p/m_B(m_t)$ . Changing variables again to  $x$  and  $y$  in Eq. (41) and using Eq. (8), we find

$$F(m) \propto m^{5/3+(1+\beta)(1-\alpha)} \int_0^1 dx x^{-8/3-(1+\beta)(1-\alpha)} \int_0^\infty dy y^{-\alpha} f(x, y). \quad (43)$$

The mass flux is independent of mass if

$$\alpha = \frac{\beta + 8/3}{\beta + 1}, \quad (44)$$

which was derived by O’Brien & Greenberg (2003) and Kobayashi & Tanaka (2010), and the reader is again referred to Appendix A for the conditions under which the integrals in Eq. (43) converge. The arguments of Pan & Sari (2005) are analogous to the calculations of O’Brien & Greenberg (2003) and Kobayashi & Tanaka (2010), but their qualitative nature has rid them of the need to worry about the scaling of  $m_0$  with  $m_t$ . We will subsequently call a fragmentation model with  $m_{0,B} = Cm_t$  and  $\beta \neq 1$  an “OBG model”.

### 3.3. Failure of the power law solution.

We now demonstrate that the power law solution (1) does not in general make the mass flux completely independent of  $m$  for any  $\alpha$ , unless  $m_{0,B} \propto m_t$  as in §3.1,3.2. To make the calculations tractable, we assume a power law dependence for  $m_B$  in the form given by Eq. (36), and for  $m_{0,B}$  in the form given by Eq. (37).

Using Eq. (41), we make the definitions

$$F_{rem}(m) \propto \int_m^\infty dm_t m_t^{5/3-\alpha} \int_0^\infty dm_p m_p^{-\alpha} f_{rem}(z, y) \quad (45)$$

$$F_{ej}(m) \propto \int_m^\infty dm_t m_t^{5/3-\alpha} \int_0^\infty dm_p m_p^{-\alpha} f_{ej}(x, y), \quad (46)$$

where  $F = F_{rem} + F_{ej}$ . Because  $x \neq z$ , in contrast to the Dohnanyi and OBG models, we change variables to  $z$  and  $y$  for the remnant flux and to  $x$  and  $y$  for the ejecta flux. This yields

$$F_{rem}(m) \propto m^{5/3+(1+\beta)(1-\alpha)} \int_0^1 dz z^{-8/3-(1+\beta)(1-\alpha)} \int_0^\infty dy y^{-\alpha} f_{rem}(z, y) \quad (47)$$

$$F_{ej}(m) \propto m^{\mu^{-1}(5/3+(1+\beta)(1-\alpha))} \int_0^{m/m_{0,B}(m)} dx x^{-1-\mu^{-1}(5/3+(1+\beta)(1-\alpha))} \int_0^\infty dy y^{-\alpha} f_{ej}(x, y). \quad (48)$$

As before,  $\alpha$  is given by Eq. (44) in order for the  $m$  dependence outside both of the integrals to vanish. Now, however,  $m$  appears in the upper limit of integration in the integral over  $x$  in the expression for  $F_{ej}$ , and unless  $m_{0,B}(m) \propto m$  (i.e.  $\mu = 1$ ),  $F(m)$  is *not* independent of  $m$ . This is one of the key conclusions of this work, and in the rest of the paper we will investigate the non-power law behavior of fragmentation cascades in detail.

To keep things simple, we will assume that the mass flux from remnants is negligible so that  $F(m) = F_{ej}(m)$ . This is consistent with Fig. 3 of Kobayashi & Tanaka (2010), which shows that  $F_{ej}/F_{rem} \sim 10$  when  $Q_D^*$  is constant.

## 4. Non-Power Law Behavior

From Eq. (48) we see that the mass flux corresponding to the power law solution of the OBG model depends only weakly (logarithmically) on  $m$ . This motivates us to look for a solution of Eq. (16) in the form

$$n(m) \propto m^{-\alpha} \varphi(m), \quad \alpha = \frac{\beta + 8/3}{\beta + 1} \quad (49)$$

where  $\varphi(m)$  is a slowly varying function of  $m$ :

$$\left| \frac{d\varphi}{dm} \right| \ll \left| \frac{\varphi}{m} \right|. \quad (50)$$

This property can be verified a posteriori, after the explicit form of  $\varphi(m)$  is obtained.

With  $n(m)$  given by Eq. (49), Eq. (41) becomes

$$F(m) \propto \int_m^\infty dm_t m_t^{5/3-\alpha} \varphi(m_t) \int_0^\infty dm_p m_p^{-\alpha} \varphi(m_p) f_{ej}(x, y). \quad (51)$$

As discussed in Appendix A, the value of  $y^{-\alpha} f_{ej}(x, y)$  typically drops off below  $y \lesssim k$  and above  $y \gtrsim k$ , which means that  $m_p^{-\alpha} f_{ej}(x, y)$  is peaked at  $m_p \sim km_B(m_t)$ , where  $k$  is a constant. In the case when erosion is neglected  $k \sim 1$ , since collisions with projectiles of mass  $m_p < m_B$  contribute no mass flux, but if erosion is included, then  $k \ll 1$  (Fig. 6 of Kobayashi & Tanaka (2010)). Together with the condition that  $\varphi(m)$  is a slowly varying function of  $m$  (Eq. (50)), this allows us to expand  $\varphi(m_p)$  in a Taylor series about  $m_p = km_B(m_t)$ :

$$\varphi(m_p) \approx \varphi(km_B(m_t)) + \frac{d\varphi}{d \ln m_p} \Big|_{m_p=km_B(m_t)} \ln \left( \frac{m_p}{km_B(m_t)} \right). \quad (52)$$

With this approximation, the inner integral of Eq. (51) becomes

$$\varphi(km_B(m_t)) \int_0^\infty dm_p m_p^{-\alpha} \varphi(m_p) f_{ej}(x, y) \left[ 1 + \frac{d \ln \varphi}{d \ln m_p} \Big|_{m_p=km_B(m_t)} \ln \left( \frac{m_p}{km_B(m_t)} \right) \right]. \quad (53)$$

From Eq. (50),  $|d \ln \varphi / d \ln m| \ll 1$ , so as long as the peak in  $m_p^{-\alpha} f_{ej}(x, y)$  at  $m_p = km_B(m_t)$  is sharp enough that  $\ln(m_p/km_B(m_t)) \sim 1$  over the width of the peak, then the second term is negligible in comparison with the first. Thus, up to terms of order  $d \ln \varphi / d \ln m$ , Eq. (51) becomes

$$F(m) \propto \int_m^\infty dm_t m_t^{5/3-\alpha} \varphi(m_t) \varphi(km_B(m_t)) \int_0^\infty dm_p m_p^{-\alpha} f_{ej}(x, y). \quad (54)$$

Changing the inner variable of integration from  $m_p$  to  $y$ , using the value of  $\alpha$  from Eq. (49), and using the definition of  $m_B(m_t)$  from Eq. (36), we have

$$F(m) \propto \int_m^\infty dm_t m_t^{-1} \varphi(m_t) \varphi(km_B(m_t)) \int_0^\infty dy y^{-\alpha} f_{ej}(x, y). \quad (55)$$

Finally, defining

$$f_{ej}(x) \equiv \int_0^\infty dy y^{-\alpha} f_{ej}(x, y), \quad (56)$$

and introducing the auxiliary function

$$\Theta(m_t) \equiv \varphi(m_t)\varphi(km_B(m_t)). \quad (57)$$

we arrive at

$$F(m) \propto \int_m^\infty dm_t m_t^{-1} \Theta(m_t) f_{ej}(x) \quad (58)$$

with  $x$  given by Eq. (22). Equation (58) is the master equation for the two-step determination of  $\varphi(m)$ :

- First, given the explicit form of  $f_{ej}(x)$  one needs to solve this integral equation under the assumption  $F = \text{const}$  to determine the behavior of the auxiliary function  $\Theta(m)$ .
- Second, having obtained  $\Theta(m)$  one must solve the functional equation, Eq. (57), to determine  $\varphi(m)$ .

We now perform this procedure explicitly for two specific forms of  $f_{ej}(x)$  — monodisperse (§4.1) and power law (§4.2).

#### 4.1. Monodisperse Fragment Mass Distribution

We first consider the special case of the *monodisperse* fragment mass distribution, which puts all fragments at a single mass scale  $m_0(m_t, m_p) = m_{0,B}(m_t)$ :

$$g_{ej}(m_f, m_t) = \frac{m_t}{m_{0,B}(m_t)} \delta(m_f - m_{0,B}(m_t)). \quad (59)$$

This singular fragmentation model can be thought of as a very crude qualitative approximation to any fragmentation law that has most of the debris mass concentrated at one scale. It allows us to obtain some interesting analytical results and serves as a simple stepping stone for the more general case considered in §4.2.

The fragmentation law (59) implies

$$f_{ej}(x) = \begin{cases} 0, & x < 1 \\ 1, & x > 1 \end{cases}, \quad (60)$$

where  $x = m/m_{0,B}(m_t)$  (§2.2). Plugging this into the master equation (Eq. (58)) one obtains

$$F(m) \propto \int_m^{\tilde{m}_{0,B}(m)} \frac{dm_t}{m_t} \Theta(m_t), \quad (61)$$

where  $\tilde{m}_{0,B}(m)$  is a new function defined as a function inverse  $m_{0,B}(m)$  (i.e.  $m_{0,B}(\tilde{m}_{0,B}(m)) = m$ ). Upon differentiation with respect to  $m$ , expression (61) results in

$$\frac{\Theta(m)}{m} = \frac{\Theta(\tilde{m}_{0,B}(m))}{\tilde{m}_{0,B}(m)} \frac{d\tilde{m}_{0,B}(m)}{dm}, \quad (62)$$

where we have used the fact that  $F(m)$  is constant. This functional equation is valid for arbitrary  $m_{0,B}(m_t)$  provided that the fragmentation law is monodisperse.

We now focus on  $\tilde{m}_{0,B}(m)$  in the form

$$\tilde{m}_{0,B}(m) = \left(\frac{m}{C}\right)^{1/\mu}, \quad (63)$$

which is valid for  $m_{0,B}$  given by Eq. (37). Plugging this expression into (62) we find

$$\Theta(m) = \frac{1}{\mu} \Theta\left(\left(\frac{m}{C}\right)^{1/\mu}\right). \quad (64)$$

Introducing the new variable  $t \equiv \ln(m^{1-\mu}/C) = \ln(m/m_{0,B}(m))$  and the new function<sup>4</sup>  $\Theta_1(t) \equiv \Theta\left((Ce^t)^{1/(1-\mu)}\right)$ , Eq. (64) becomes

$$\Theta_1(t) = \frac{1}{\mu} \Theta_1\left(\frac{t}{\mu}\right). \quad (65)$$

This has the form of a homogeneous functional equation

$$q(au) = bq(u), \quad (66)$$

( $a$  and  $b$  are constants) which has the solution

$$q(u) = T(\ln u)u^\lambda, \quad \lambda \equiv \frac{\ln b}{\ln a}. \quad (67)$$

Here  $T(s) = T(s + \ln a)$  is an arbitrary periodic function with period  $\ln a$ , which can be constant (Polyanin & Manzhirov, 1998). This implies that the solution of Eq. (65) is

$$\Theta_1(t) = \frac{T(\ln t)}{t}, \quad (68)$$

so that finally

$$\Theta(m) = \frac{T(\ln(\ln(m/m_{0,B}(m))))}{\ln(m/m_{0,B}(m))}, \quad T(s) = T(s + \ln \mu). \quad (69)$$

Clearly this solution is inapplicable to the OBG case of  $\mu = 1$ , because the variable  $t$  then reduces to a constant. However, for  $\mu = 1$ , Eq. (64) already has the form (66), so that its solution is

$$\Theta(m) = T(\ln m), \quad T(s) = T(s + \ln C). \quad (70)$$

---

<sup>4</sup>We are grateful to Jeremy Goodman for suggesting this transformation.

In particular,  $\Theta(m)=\text{const}$ , and consequently  $\varphi(m)=\text{const}$ , is one of the possible solutions, so that  $n(m)$  simply proportional to  $m^{-\alpha}$  with  $\alpha$  given by (44) is a viable solution for a fragmentation cascade with  $\mu = 1$ , in agreement with O’Brien & Greenberg (2003).

However, the existence of periodic solutions brings about the possibility of having *waves* in the mass distribution of objects while still having  $F(m)$  constant, even for  $\mu = 1$ . The presence of waves at masses  $m/m_{rm} \sim 1$  in fragmentation cascades having a lower mass cutoff has been previously demonstrated by Campo Bagatin et al. (1994), Durda & Dermott (1997), and Thébault & Augereau (2007); O’Brien & Greenberg (2003) found waves to appear whenever the scaling of specific energy necessary for disruption  $Q_D^*$  with object mass changed abruptly (e.g. due to an object’s self-gravity becoming more important than its internal strength); and Fraser (2009), Pan & Sari (2005), and Kenyon & Bromley (2004) have shown waves to be present at the transition from a collisionally evolved to a primordial size distribution (i.e. at  $m/m_{inj} \sim 1$ ).

The nature of the waves we have found is different from the ones discussed by previous authors, since they exist even when  $m_{rm} = 0$ ,  $m_{inj} = \infty$ , and  $m_B$  is given by a pure power law without breaks (Eq. (36)). In astrophysical systems, these kinds of waves could be triggered in stochastic collisions of large planetesimals (Kenyon & Bromley, 2005; Wyatt & Dent, 2002; Wyatt, 2008). Most of the mass in such a collision would be in particles of size  $m_0(m_t, m_p)$ , and if the density of particles with mass  $m_0$  created in the collision is comparable to or exceeds the local disk density of such particles, a wave will be triggered. However, a proper treatment of these waves needs to account for a non-monodisperse fragment mass distribution, which could damp them, so we leave this subject for future work (Belyaev & Rafikov, in preparation).

## 4.2. Power Law Fragment Mass Distribution

We now assume that the mass spectrum of fragments produced in a collision  $g_{ej}(m_f, m_t, m_p)$  is a power law with an index  $-\eta$  having a cutoff at a maximum fragment mass  $m_0(m_t, m_p) = m_{0,B}(m_t)$ . This allows us to write

$$f_{ej}(x) = \begin{cases} x^{2-\eta}, & x < 1 \\ 1, & x > 1 \end{cases}, \quad (71)$$

where as before  $x = m/m_{0,B}(m_t)$  (§2.2). This fragmentation model resembles reality, since observational and experimental evidence (Gault & Wedekind, 1969; Fujiwara et al., 1977) as well as numerical simulations (Benz et al, 1994; Benz & Asphaug, 1999) suggest power law behavior of  $g_{ej}(m, m_t, m_p)$  at small fragment masses (§2.2). Various flavors of such a power law model have been adopted in theoretical studies by Dohnanyi (1969), Williams & Wetherill (1994), O’Brien & Greenberg (2003), Kenyon & Bromley (2010), Davis & Farinella (1997), Kobayashi & Tanaka (2010), etc.

Plugging Eq. (71) into the master equation (Eq. (58)), we find

$$F(m) \propto \int_m^{\tilde{m}_{0,B}(m)} \frac{dm_t}{m_t} \Theta(m_t) + \int_{\tilde{m}_{0,B}(m)}^{\infty} \frac{dm_t}{m_t} \left[ \frac{m}{m_{0,B}(m_t)} \right]^{2-\eta} \Theta(m_t). \quad (72)$$

Differentiating this expression with respect to  $m$  (keeping in mind that  $dF(m)/dm = 0$ ), dividing the resultant expression by  $m^{1-\eta}$ , and differentiating again one finds

$$\frac{d \ln \tilde{m}_{0,B}(m)}{d \ln m} \Theta(\tilde{m}_{0,B}(m)) = \Theta(m) - \frac{1}{2-\eta} \frac{d\Theta(m)}{d \ln m}. \quad (73)$$

This equation reduces to Eq. (62) if one takes the limit  $\eta \rightarrow -\infty$  which corresponds to all of the fragments' mass concentrated in objects with mass  $m_{0,B}$ , and is thus equivalent to a monodisperse fragmentation law.

Until now, our treatment was rather general and based solely on assumption (71) so that the functional equation (73) is valid for any form of  $m_{0,B}$ . We now take  $m_{0,B}$  in the form of Eq. (37) and find

$$\frac{\Theta(\tilde{m}_{0,B}(m))}{\mu} = \Theta(m) - \frac{1}{2-\eta} \frac{d\Theta(m)}{d \ln m}. \quad (74)$$

In the limit  $\eta \rightarrow -\infty$ , corresponding to the monodisperse case, the second term on the right hand side of (74) is zero, and the solution is easily verified to be

$$\Theta(m) = \frac{1}{\ln(m/m_{0,B}(m))}. \quad (75)$$

This solution could also have been obtained from Eq. (69) by setting  $T = 1$ .

For the non-monodisperse case, we can solve Eq. (74) by first introducing a new independent variable  $w \equiv 1/\ln(m/m_{0,B}(m))$ , and the new function  $\Theta_1(w) = \Theta(m) = \Theta((Ce^{1/w})^{1/(1-\mu)})$ . This is a natural choice, since  $\Theta(m) = w$  is the exact solution for the monodisperse case if  $T(\ln(\ln(m/m_{0,B}(m)))) = 1$ . With these definitions we can rewrite Eq. (74) as

$$\frac{\Theta_1(\mu w)}{\mu} = \Theta_1(w) - \frac{\mu-1}{2-\eta} w^2 \frac{d\Theta_1(w)}{dw}. \quad (76)$$

We next look for the solution of this equation in the form of an infinite series

$$\Theta_1(w) = \sum_{k=1}^{\infty} A_k w^k \quad (77)$$

(note that  $A_0 = 0$  as long as  $\mu \neq 1$ ). By plugging this ansatz into Eq. (76) and changing the index of summation in the last term we get

$$\sum_{k=1}^{\infty} A_k \mu^{k-1} w^k = \sum_{k=1}^{\infty} A_k w^k + \frac{1-\mu}{2-\eta} \sum_{k=2}^{\infty} (k-1) A_{k-1} w^k. \quad (78)$$



We can set  $A_1$  equal to any value and this corresponds to an overall normalization of  $\Theta_1$ . We then obtain the other coefficients from the recursive relation

$$A_{k+1} = \frac{(1-\mu)k}{(2-\eta)(\mu^k-1)}A_k, \quad k = 1, \dots, \infty. \quad (79)$$

Unfortunately, this series only converges for  $\mu > 1$ .

For  $\mu < 1$ , we have found numerically in §5.1.1 that the formula

$$\Theta(m) = \frac{1}{\ln(m/m_{0,B}(m)) + 1/(2-\eta)} \quad (80)$$

gives good results up to  $\eta \lesssim 1.7$ . Equation (80) is a version of the monodisperse solution (75), which has been shifted in  $\ln m$ , and is accurate up to terms of  $O(w^3)$  in Eq. (78).

## 5. Numerical verification of non-power law behavior

Having obtained solutions for  $\Theta(m)$  for a couple of fragmentation models, we are now in a position to determine  $\varphi(m)$  from Eq. (57). The analytical calculations involved in this process are rather cumbersome and we refer the interested reader to Appendix B for the mathematical details. There, we describe the general method of solving for  $\varphi(m)$  which works for  $m_B$  given by Eq. (36) and for arbitrary  $\Theta(m)$ . However, we provide explicit analytical results only for  $\Theta(m)$  corresponding to the monodisperse case in Appendix B.3. In this section, we compare these analytical results with numerical calculations of fragmentation cascades. The latter were carried out using a fragmentation code which is described in detail in Appendix C. For simplicity, we ignore erosion in our calculations, which amounts to setting  $k = 1$  in Eq. (57).

### 5.1. Results for $\mu \neq 1$ and $m_B(m) = m$ .

As discussed in §2.1, real astrophysical systems typically have  $m_B(m_t) \ll m_t$ . In order to *qualitatively* understand the non-power law behavior, however, it is instructive to consider a simplified model in which there is no erosion. Next, we also assume that a target can only be broken by projectiles that are of very nearly the same size as itself:

$$m_B(m_t) = (1 - \epsilon)m_t, \quad \epsilon \ll 1. \quad (81)$$

Although such an assumption is unrealistic, it is useful for getting a qualitative picture of the non-power law behavior.

In the model we have just introduced, which we will call the  $m_B = m$  model, the analog of Eq. (51) is

$$F(m) \propto \int_m^\infty dm_t m_t^{5/3-\alpha} \varphi(m_t) \int_{m_B(m_t)}^{\tilde{m}_B(m_t)} dm_p m_p^{-\alpha} \varphi(m_p) f_{ej}(x, y), \quad (82)$$

where  $\tilde{m}_B(m)$  is defined to be the largest mass that can be broken by a projectile of mass  $m$  (i.e.  $m_B(\tilde{m}_B(m)) = m$ ). The power law slope of this model is  $\alpha = 11/6$  just like the Dohnanyi case, and it is straightforward to show that the master equation (Eq. (58)) and Eq. (57) are both still valid for the  $m_B = m$  model. Now, however, Eq. (57) is trivial to solve, since we have  $m_B(m_t) \approx m_t$ , which implies that  $\varphi(m) \approx \sqrt{\Theta(m)}$ . Comparison between the numerical and analytical behavior of  $\varphi(m)$  then becomes a direct verification of our solutions for  $\Theta(m)$  obtained in §4, and we avoid the intermediate steps involved in solving Eq. (57) for arbitrary  $m_B$ .

In our numerical calculations we implement the case of  $m_B(m_t) = m_t$  by taking  $m_B(m_t) = 0.99m_t$ . We specify the amount of time for which simulation was run in one of two ways, but both make use of the collision time defined generally as

$$\tau_c(m_t, t) \equiv \left[ \left( \frac{3}{4\pi\rho} \right)^{2/3} \pi v \int_{m_B(m_t)}^{\tilde{m}_B(m_t)} dm_p n(m_p, t) \left( m_p^{1/3} + m_t^{1/3} \right)^2 \right]^{-1}. \quad (83)$$

Here, we have assumed a geometric cross-section for collisions and mass-independent relative velocities as in §2.1. First, we can specify how long a simulation was run in terms of the number of collision times of the smallest particles in the simulation. This is a natural unit of measure to use, since this is the timescale on which the low mass end of the particle mass distribution evolves, unless the initial distribution is already in a steady-state. Second, we can specify how long a simulation was run by the location of the collisional break,  $m_{break}$ , at the end of the simulation,  $t = t_{end}$ , which is given implicitly by  $\tau_c(m_{break}, t_{end}) = t_{end}$ . The quantity  $m_{break}$  is especially useful when interpreting simulation results for which the distribution was initialized to be in a steady-state to check an analytical steady-state solution (§5.1.2 and 5.2). In this case, there should be no evolution of the distribution in time, and so no break should develop. However,  $m_{break}$  gives the mass below which we *would have seen* evolution, if the analytical steady-state solution were incorrect.

### 5.1.1. Monodisperse Fragment Mass Distribution.

We first consider the ansatz (81) with  $\mu \neq 1$  and the monodisperse fragment mass distribution. Using Eq. (69) we find

$$\varphi(m) = \frac{1}{\sqrt{\ln(m/m_{0,B}(m))}}, \quad (84)$$

where we have set the arbitrary periodic function  $T$  to a constant.

To verify Eq. (84) numerically, we initialize a pure power law mass distribution  $n_0(m) \propto m^{-\alpha}$  with an index  $\alpha = 11/6$ , which is the steady-state solution of the Dohnanyi model. We then expect that for  $\mu \neq 1$  the shape of  $n(m, t)$  will gradually evolve from  $n_0(m)$  towards the correct solution (49) with  $\varphi(m)$  given by Eq. (84). To illustrate this evolution in Fig. 1 and all subsequent figures, we plot the “effective population index”  $\alpha_{eff}(m, t) \equiv -d \ln n(m, t) / d \ln m$  as a function of  $m$  at different moments of time. This way of representing the evolution of  $n(m, t)$  naturally highlights

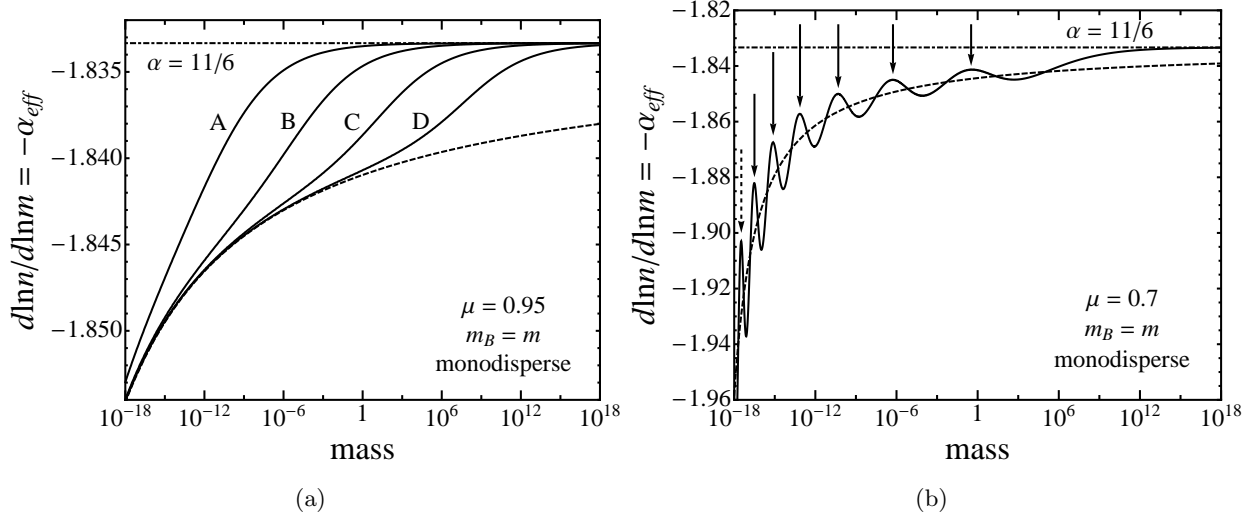


Fig. 1.— Population index  $d \ln n / d \ln m = -\alpha_{eff}$  of the particle mass distribution vs. mass for two different values of  $\mu$  in the relation  $m_{0,B} = C m_t^\mu$ . Both panels display the evolution of  $\alpha_{eff}$  for  $m_B(m) = m$  starting from an initial distribution  $n_0(m) \propto m^{-11/6}$  (the Dohnanyi model). Panel (a) shows the smooth convergence of  $n(m, t)$  from  $n_0(m)$  to the solution  $n(m) = m^{-\alpha} \varphi(m)$ , with  $\varphi(m)$  given by Eq. (84) and shown by the dashed line. The model parameters are  $m_B(m) = m$ ,  $\mu = 0.95$ , and  $m_{0,B}(m = 10^{-18}) = 0.3m$  (mass scale is arbitrary), which sets  $C$  in the expression for  $m_{0,B}$ . The curves A-D show the solution after 25, 250, 2500, and 25000 collision times (defined in §5.1) of particles with mass  $m = 10^{-18}$ . Panel (b) shows the numerical solution starting again from a Dohnanyi distribution as in panel (a), but with  $\mu = 0.7$  and all other parameters the same. The simulation was run for 5000 collision times of particles with mass  $m = 10^{-18}$ . The numerical solution (solid line) no longer converges smoothly to the analytic solution (84) (dashed line), but oscillates about it. Given the location of the leftmost peak (dashed arrow), Eq. (69) correctly predicts the locations of the other peaks as indicated by the solid arrows.

the non-power law behavior, since  $\alpha_{eff}$  for  $n$  given by a power law as in Eq. (1) appears as the horizontal line  $\alpha_{eff} = \alpha$  in such plot. Thus, any deviation from a horizontal line is indicative of non-power law scaling of  $n(m)$ .

In Fig. 1a, we display the case of  $\mu$  close to unity ( $\mu = 0.95$ ), which according to (84) corresponds to an almost constant  $\varphi$  since  $m/m_{0,B}(m) \propto m^{0.05}$ ; note the small range of variation of  $\alpha_{eff}$  in Fig. 1a. For this value of  $\mu$  we indeed find that the initial power law distribution smoothly converges to the analytic solution (84) over time.

In Fig. 1b, we show the evolution of  $\alpha_{eff}$  for  $\mu = 0.7$ , appreciably different from  $\mu = 1$ . One can see that in this case the numerical solution does not converge towards the analytical solution in a smooth fashion. Instead the numerical solution *oscillates* in mass space about the analytical solution. The frequency of these oscillations is correctly predicted by Eq. (69), and the positions of

the peaks computed according to this formula are shown by the arrows in Fig. 1b. Their agreement with the locations of numerical peaks proves that waves can indeed be spontaneously generated and persist with no indication of damping in smooth fragmentation models (i.e. for functions  $m_B$  and  $m_0$  not having any breaks caused by the abrupt changes of the material properties of colliding objects), at least for a monodisperse fragment mass distribution.

In this study, the appearance of waves is undesirable as it complicates the comparison between numerical and analytical solutions for  $n(m)$ , and one would like to avoid their excitation. Comparing the two cases depicted in Fig. 1 suggests that waves get generated when the initial distribution  $n_0(m)$  is significantly different from the analytical, non-oscillatory steady-state solution. Motivated by this observation, we start from an initial distribution  $n_0(m)$  which is *identical* to the analytical steady-state solution in subsequent calculations. We then expect that the numerical solution,  $n(m, t)$ , will not deviate from  $n_0(m)$  as time goes by if our steady-state solution is correct; if it is not, then  $n(m, t)$  will evolve away from  $n_0(m)$ .

Despite the complications related to the appearance of waves, it is clear that in the monodisperse case,  $n(m)$  exhibits non-power law behavior for  $\mu \neq 1$ , and our analytical solutions (69) and (84) accurately describe the deviation from the pure power law solution.

To better understand the qualitative behavior of the steady-state  $\alpha_{eff}(m)$  in Fig. 1, we use Eq. (37), Eq. (49), and Eq. (84) to write

$$\alpha_{eff} = \alpha + \frac{1}{2 \ln(m/m_0^*)}, \quad (85)$$

where  $m_0^* = C^{1/(1-\mu)}$  is the mass scale at which the mass of the largest fragment becomes formally equal to the mass of the target (i.e.  $m_{0,B}(m_0^*) = m_0^*$ ). For  $\mu < 1$  a fragmentation cascade can only exist for  $m > m_0^*$ , in which case  $\alpha_{eff} > \alpha$ , as can be seen in Fig. 1 ( $\alpha = 11/6$ , since  $\beta = 1$  for  $m_B = m$ ). Thus, in the monodisperse case with  $m_B = m$ , the  $\mu < 1$  collisional mass spectrum is *steeper* than in the Dohnanyi model. The deviation of  $\alpha_{eff}$  from the Dohnanyi slope increases as  $m \rightarrow m_0^*$ , and decreases for  $m \gg m_0^*$ . For example, in the case shown in Fig. 1b one has  $m_0^* = 1.8 \times 10^{-20}$  and  $\alpha_{eff}$  deviates from 11/6 by  $\approx 0.12$  already at  $m = 10^{-18}$ , i.e. at  $m/m_0^* \sim 55$ .

On the contrary, in the monodisperse case with  $\mu > 1$ , a fragmentation cascade is possible only for  $m < m_0^*$ , and Eq. (85) then predicts that  $\alpha_{eff} < \alpha$ . Thus, the collisional mass spectrum for  $\mu > 1$  has a *shallower* slope than the Dohnanyi solution. This can be seen in Fig. 2a (curve labeled “ $-\infty$ ”), Fig. 3b (dotted curve), and Fig. 4a (dotted curve). In that case, the biggest deviations of  $\alpha_{eff}$  from  $\alpha$  are observed at large masses, as  $m \rightarrow m_0^*$ .

### 5.1.2. Power Law Fragment Mass Distribution

We now consider ansatz (81) with the power law fragment mass distribution explored in §4.2. In this case,  $\varphi(m)$  is given exactly as the square root of Eq. (78) for  $\mu > 1$ , and approximately

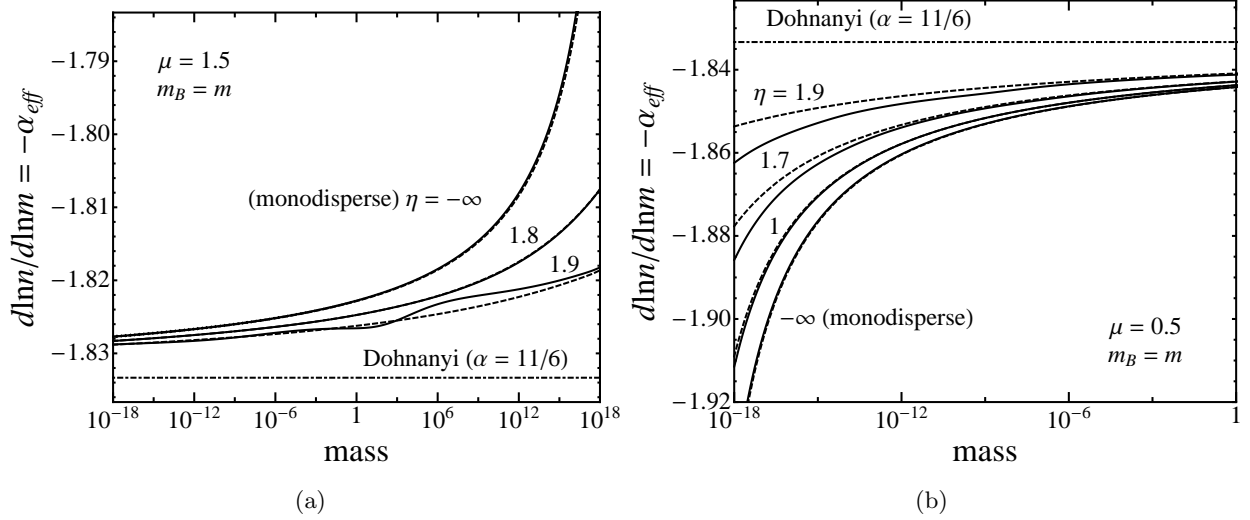


Fig. 2.— Population index of the mass distribution vs. mass for a power law fragment mass distribution and two different values of  $\mu$ .  $n_0(m)$  was initialized to be the analytical steady-state solution for each model. The dot-dashed line indicates the  $\alpha = 11/6$  “Dohnanyi” power law index which would be expected for the  $\mu = 1$  case. The labels in each panel indicate the value of power law index  $\eta$  of the fragment mass distribution for different models, and a monodisperse model (corresponding to  $\eta = -\infty$ ) is plotted for reference (its behavior is given by Eq. (84)). Panel (a): The numerical calculations were compared with the analytic series solution (Eq. (78)) truncated after 20 terms. Curves for two models both having  $m_B(m) = m$ ,  $\mu = 1.5$ ,  $m_{0,B}(m = 10^{18}) = 0.1m$ , and either  $\eta = 1.8$  or  $1.9$  are shown. The analytic solutions (dashed lines) agree well with numerical runs (solid lines), although there is some deviation for the  $\eta = 1.9$  case. The location of  $m_{\text{break}}$  (§5.1) in the simulations is  $m_{\text{break}} \sim 10^3$ . Panel (b): Similar to panel (a), but now the approximate solution (Eq. (80)) was computed for three models, each having  $m_B(m) = m$ ,  $\mu = 0.5$ ,  $m_{0,B}(m = 10^{-18}) = 0.1m$ , and either  $\eta = 1, 1.7$ , or  $1.9$ . There is good agreement between the analytic solutions (dashed line) and numerical results (solid lines) for  $\eta \lesssim 1.7$ . Here  $m_{\text{break}} = 10^5$ , although we have truncated the mass range at  $m = 1$  to highlight the differences between the solutions.

as the square root of Eq. (80) for  $\mu < 1$ . We again test these solutions numerically, but this time starting with the analytical steady-state mass distribution (as discussed in the previous section), since we are not interested in waves.

For the  $\mu > 1$  case, we find that the solution given by the the series in Eq. (78) converges quickly, and truncating the series after the first twenty terms gives a result which shows little sign of evolution for  $\eta = 1.8$ , (Fig. 2a). Since in the  $\eta = 1.8$  case numerical  $n(m, t)$  does not evolve significantly from the initial distribution given by the steady-state solution (Eq. (78)), this implies that our analytic solution for  $\mu > 1$  is indeed correct, even for  $\eta$  very close to 2. In Fig. 2b

we show the analogous calculation for the  $\mu < 1$  case. We initialize  $n_0$  to be the approximate solution given by Eq. (80) and find that for  $\eta \lesssim 1.7$  this solution works well. However, for larger values of  $\eta$  deviations between the steady-state numerical and analytical solutions become apparent. Nevertheless, the general qualitative behavior is still reproduced by Eq. (80) even for  $\eta$  close to 2.

It is easy to see from Fig. 2 that as  $\eta \rightarrow 2$  the behavior of  $\alpha_{eff}$  flattens out and approaches a power law solution with slope given by Eq. (44), which is just  $\alpha = 11/6$  for  $m_B = m$ . Such behavior can be understood by looking at Eq. (74), which reduces to  $d\Theta(m)/dm = 0$ , in the limit of  $\eta \rightarrow 2$ . This means that  $\Theta(m)$  does not vary with mass in this limit, which implies that  $\varphi(m)$  is also constant if  $m_B(m) = m$ . Thus, in the limit  $\eta \rightarrow 2$  when fragments produced in an individual collision are uniformly distributed in  $\ln m$ , the steady-state solution is a power law.

On the other hand, the smaller  $\eta$  becomes, the more the fragment mass distribution  $g$  is dominated (by mass) by the largest fragments, which makes it approach a monodisperse distribution. One then expects that when  $\eta$  is reduced,  $\alpha_{eff}$  should tend towards the monodisperse form given in Eq. (85), and this trend is clearly seen in Fig. 2. It is also worth noting that for a given value of  $\mu$ , the largest deviation of  $\alpha_{eff}$  from pure power law behavior occurs for the monodisperse fragment mass distribution, which is obtained in the limit  $\eta \rightarrow -\infty$ .

## 5.2. Results for $\mu \neq 1$ and general $m_B(m)$ .

We now describe our results for the more realistic case when  $m_B \neq m_t$ .  $m_{0,B}$  is again given by Eq. (37) with  $\mu \neq 1$ , which is necessary for the non-power law behavior. The general approach developed in Appendix B allows us to compute  $\varphi(m)$  for arbitrary  $\Theta(m)$ , including that obtained in §4.2 for the power law fragment mass distribution. To keep things simple, however, we only provide a comparison between numerical and analytical results in the case of a monodisperse fragment mass distribution, for which we derived closed form analytical expressions in Appendix B.

We start by looking at the case of  $\beta = 1$ , so we have  $m_B(m) = Bm$ ,  $B < 1$ . For a given set of parameters, we initialize  $n_0(m)$  to be the analytical steady-state solution given by Eq. (B23) if  $\mu > 1$  or by Eq. (B25) if  $\mu < 1$ . We then check whether  $n(m, t)$  evolves away from  $n_0(m)$ . If it does not, then  $n_0(m)$  is the steady-state solution.

In Fig. 3a we compare the analytical formula (B25) for  $\mu = 0.5$  with the numerical solution. Despite small deviations between the two solutions (likely due to some problems with boundary conditions, see Appendix C, and, possibly, weak wave excitation) the overall agreement between them is quite good. Figure 3b provides a comparison between our formula (B23) for  $\mu = 1.5$  and the numerical solution. In this case, the two solutions agree with each other so well that they are hard to distinguish.

We next look at the case of  $\mu \neq 1$  and  $\beta \neq 1$ , so that  $m_B$  is given by Eq. (36). Proceeding as before, we display in Fig. 4 the evolution of numerical curves for  $\alpha_{eff}$  away from analytical

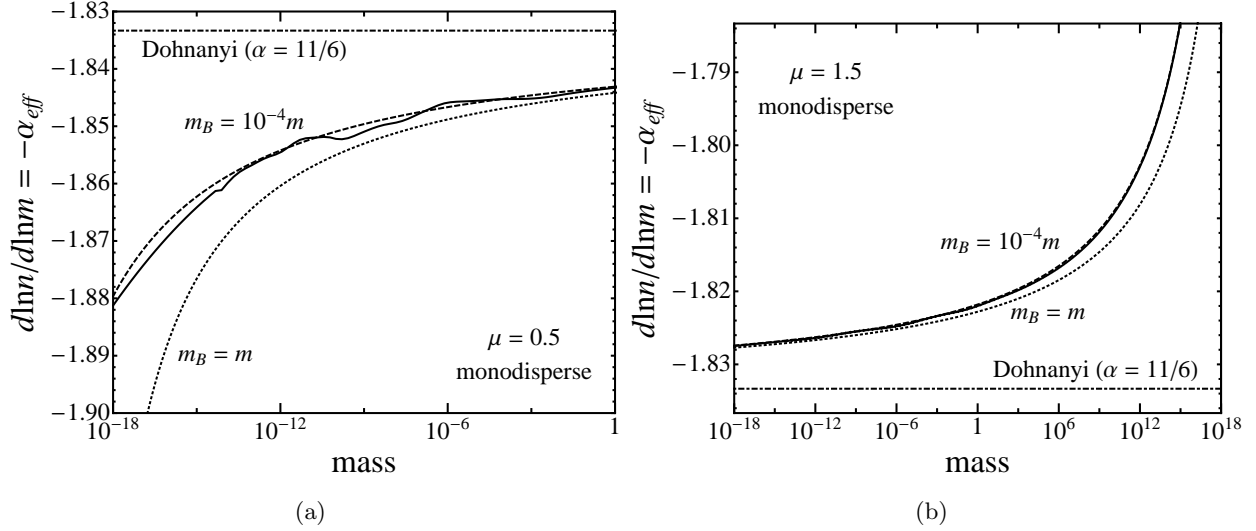


Fig. 3.— Population index of the mass distribution vs. mass for  $m_B(m) = Bm$ ,  $B = 10^{-4}$ , and two different values of  $\mu$ .  $n_0(m)$  was initialized to be the analytical steady-state solution for each model. The dot-dashed line indicates the  $\alpha = 11/6$  “Dohnanyi” power law index which would be expected for the  $\mu = 1$  case. The dotted line represents the monodisperse solution with  $m_B(m) = m$ . Panel (a): Analytic solution (B25), (dashed line) is compared with the numerical result (solid line) for a monodisperse fragmentation model having  $\mu = 0.5$ , and  $m_{0,B}(m = 10^{-18}) = 0.1m$ . The location of  $m_{break}$  is at  $m_{break} \sim 0.01$ . The effect of the imposed boundary conditions (Appendix C) is evident as the straight line between  $m = 10^{-14} - 10^{-18}$ . Panel (b): Similar to panel (a), but now the analytic solution (B23) was computed for a model with  $\mu = 1.5$ , and  $m_{0,B}(m = 10^{18}) = 0.1m$ . The dashed and solid lines are hard to distinguish here because the numerical solution does not significantly evolve away from the initial analytical solution. The value of  $m_{break}$  is  $m_{break} = 10^7$ .

solutions computed in Appendix B.3.2. The panels in this figure show our results for  $\beta < 1$ ,  $\mu > 1$  and  $\beta > 1$ ,  $\mu < 1$ . We do not show the results for  $\beta > 1$ ,  $\mu > 1$  and  $\beta < 1$ ,  $\mu < 1$  due to numerical difficulties with imposing boundary conditions in these two cases (Appendix C). The agreement between the analytical formula (B27) for  $\beta < 1$  and the numerical results displayed in Fig. 4a is quite good, and the same is true regarding the agreement between the formula (B26) for  $\beta > 1$  and the numerical results displayed in Fig. 4b.

In both Fig. 3 and Fig. 4, we display  $\alpha_{eff}$  computed for  $m_B = m$  and a monodisperse fragment size distribution (§5.1.1) by a dotted line. One can see that even though we are now using  $m_B \ll m$ , the solutions are qualitatively similar to the  $m_B = m$  case. Thus, one can use the fully analytic solution (49) with  $\varphi(m)$  given by Eq. (84) to get a qualitative picture of the non-power law behavior regardless of the precise form of  $m_B$ . We also note that the solutions for  $\alpha_{eff}$  shown in Fig. 3 and Fig. 4 lie *above* the solution corresponding to the  $m_B = m$  case. Thus,  $m_B \neq m$  gives rise to a function  $\varphi(m)$  which is *shallower* than for the  $m_B = m$  case.

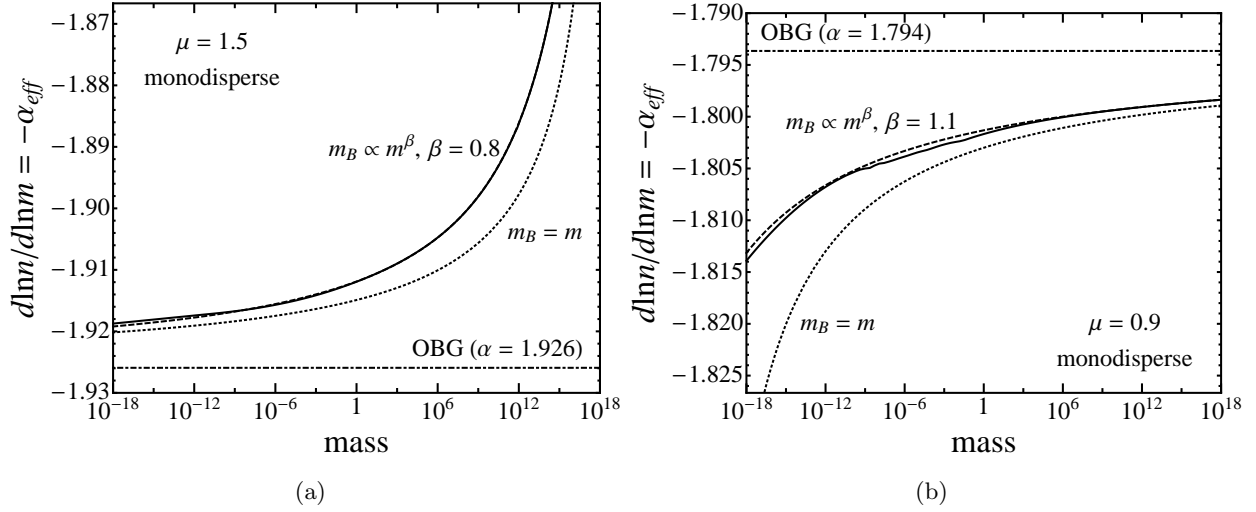


Fig. 4.— Population index of the mass distribution vs. mass for the cases  $\beta < 1$ ,  $\mu > 1$  and  $\beta > 1$ ,  $\mu < 1$ . Calculations were initialized at the analytical steady-state solution for each model. The dot-dashed line indicates the  $\alpha$  given by Eq. (44) — the OBG power law index which would be expected for the  $\mu = 1$ ,  $\beta \neq 1$  case. The dotted line represents the monodisperse solution with  $m_B(m) = m$ . Panel (a): The analytic solution (B27) (dashed line) is compared with the numerical result (solid line) for a monodisperse fragmentation model with  $\beta = 0.8$ ,  $\mu = 1.5$ ,  $m_{0,B}(m = 10^{18}) = 0.1m$ , and  $m_B(m = 10^{-18}) = 10^{-6}m$ . The location of the break is  $m_{\text{break}} = 10^4$ . Panel (b): Similar to panel (a), but now Eq. (B26) was used to initialize the analytic solution for  $\beta = 1.1$ ,  $\mu = 0.9$ ,  $m_{0,B}(m = 10^{-18}) = 0.03m$ , and  $m_B(m = 10^{18}) = 10^{-4}m$ . The location of the break is at  $m_{\text{break}} = 10^{-4}$ . In both panels (a) and (b), the numerical and analytical results are in agreement.

## 6. Discussion

### 6.1. Validity of $|d \ln \varphi / d \ln m| \ll 1$

In deriving our analytical results, we have assumed that  $|d \ln \varphi / d \ln m| \ll 1$  (Eq. 50). Results from the previous section demonstrate that the qualitative behavior of  $\varphi(m)$  is insensitive to the specific form of  $m_B$ . Thus we can get a sense of when this assumption is valid by using the form of  $d \ln \varphi / d \ln m$  for the monodisperse case with  $m_B = m$ :

$$\frac{d \ln \varphi(m)}{d \ln m} = -\frac{1}{2 \ln(m/m_0^*)}, \quad (86)$$

In order to have  $|d \ln \varphi / d \ln m| \ll 1$ , we must have  $|\ln(m/m_0^*)| \gg 1$ , where  $m_0^*$  was defined in §5.1.1. In practice, we find that even for  $|\ln(m/m_0^*)| \sim 4$  our analytical solutions give an accurate description of the non-power law behavior. For instance, in Fig. 2b it is clear that for the monodisperse fragmentation law, the exact solution for  $\varphi(m)$  (Eq. (84)) works very well, even though we have



$$|\ln(m/m_0^*)| = 4.6 \text{ at } m = 10^{-18}.$$

## 6.2. Comparison with existing studies

We illustrate how our work fits into existing studies of fragmentation cascades with a parameter space plot in  $\mu - \beta$  coordinates. Figure 5 shows the domains of applicability in the  $\mu - \beta$  plane for the Dohnanyi and OBG solutions in relation to our analytic solutions for the monodisperse case. Each of our solutions is labeled by its corresponding formula number, and it is evident that our investigation covers the remainder of the  $\mu - \beta$  plane.

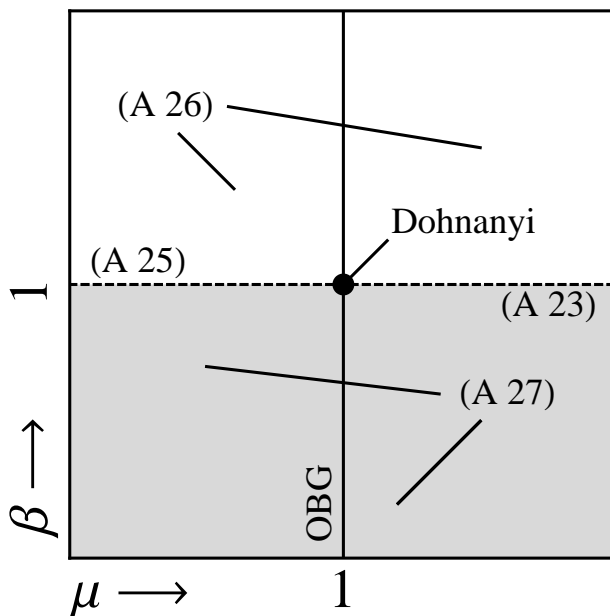


Fig. 5.— Parameter space plot in the  $\mu - \beta$  plane. The case considered by Dohnanyi (1969); Tanaka et al. (1996) is at the point  $\mu = 1, \beta = 1$ , and the case considered by O’Brien & Greenberg (2003) lies on the line  $\mu = 1$  (solid line). Our solutions cover the rest of phase space and are labeled with references to corresponding equations in this work. Thus, solutions (B25) and (B23) (monodisperse,  $m_B(m) = Bm$ ) lie on rays  $\mu < 1, \beta = 1$  and  $\mu > 1, \beta = 1$ , correspondingly. Solutions (B26) and (B27) (monodisperse,  $m_B(m) = Bm^\beta$ ) are valid in the half planes  $\beta > 1$  (white) and  $\beta < 1$  (gray) respectively. For these solutions  $\varphi = \text{const}$  along the line  $\mu = 1$  in agreement with O’Brien & Greenberg (2003).

We next discuss why previous authors have not seen non-power law behavior. The reason is that they have all assumed  $m_{0,B} \propto m_t$ , and we have shown in §3.3 that non-power law behavior only results when  $m_{0,B}$  is not proportional to  $m_t$ . In some studies, the assumption  $m_{0,B} \propto m_t$  was explicit such as in Dohnanyi (1969) and O’Brien & Greenberg (2003) who both assumed  $m_0 = Cm_t$ , and in Petit & Farinella (1993), O’Brien & Greenberg (2005), and de Elía & Brunini (2007) who

all assumed<sup>5</sup>  $m_{0,B} = m_t/2$ . In other cases, such as Tanaka et al. (1996) and Kobayashi & Tanaka (2010) the scaling  $m_{0,B} \propto m_t$  was implicit in assumptions about the form of  $f_{ej}$  (§3.1, §3.2).

We now return to our argument from §2.3 that  $m_{0,B}$  should have the form (37). This conclusion was based on an extension of the experimental results of Fujiwara et al. (1977) beyond the strength-dominated regime. We mention that a number of authors (Petit & Farinella, 1993; O’Brien & Greenberg, 2005; de Elía & Brunini, 2007) have considered a different extension of those results, and instead of our Eq. (31), these authors used

$$\frac{m_0(m_t, m_p)}{m_t} \propto \left( \frac{E_{coll}(m_t, m_p)/2}{Q_S(m_t)m_t} \right)^{-\gamma}, \quad (87)$$

Here,  $Q_S$  is the energy per unit mass required to shatter an object, but not necessarily to disperse its fragments to infinity (O’Brien & Greenberg, 2005). If we assume for simplicity that  $Q_D^* \propto Q_S$ , then from Eq. (87) and Eq. (20), we have  $m_{0,B} \propto m_t$ , for any functional form of  $m_B$ . The reason it is possible to derive two different forms for  $m_0(m_t, m_p)$  from the results of Fujiwara et al. (1977) (Eq. (31) and Eq. (87)) is because their experiments were performed over a small range of target masses using a constant projectile mass. The question of how to properly extend their results over a larger mass range can best be settled by more experiments and simulations (Stewart & Leinhardt, 2009; Benz & Asphaug, 1999; Benz et al, 1994), which can decisively answer how  $m_{0,B}$  varies with mass. However, we point out that unless  $m_{0,B}$  is exactly proportional to  $m_t$ , non-power law behavior will result. As we show in the next section, these deviations from power law behavior can be observationally significant when extrapolating over many orders of magnitude in mass.

### 6.3. Applications

Our results clearly demonstrate that one should be somewhat cautious when adopting a pure power law approximation to describe the properties of fragmentation cascades. Even though the non-power law corrections computed in this work scale very weakly with object mass (as the square root of the logarithm of the mass (Eq. (84))), one has to keep in mind that in astrophysical systems collisional cascades span  $\sim 30$  orders of magnitude in mass. Thus, even a weak deviation from a power law can become important, such as when inferring the disk mass (dominated by the largest bodies) from its infrared luminosity (dominated by the smallest bodies) (Wyatt, 2008).

Just for illustration, let us consider a population of  $R_{inj} = 10$  km objects which get ground down to  $R_{rm} = 1 \mu\text{m}$  size particles by collisions. Infrared observations give us some idea of the mass in small particles, thus fixing the normalization of the mass spectrum at its low-mass end, and we want to infer from these data the total mass in large bodies feeding this collisional cascade. Connecting the mass contained at the low and high mass ends of the spectrum by a simple power

---

<sup>5</sup>Note that  $m_{0,B} = m_t/2$  does not follow from  $m_{rem}(m_B(m_t), m_t) = m_t/2$ , because the remnant does not belong to the distribution of ejecta (§2).

law leads to an error caused by the neglect of the non-power law effects. We can estimate this error  $\delta$  by using Eq. (84) and taking the ratio of  $\varphi$  at the high and low mass ends. Assuming some values of  $\mu$  and  $C$  in Eq. (37) that are “averaged” over the whole cascade (in practice these parameters will change several times between  $R_{rm}$  and  $R_{inj}$  because of variations in the internal properties of objects), we have

$$\delta \approx \sqrt{\frac{\ln(R_{rm}/R_0^*)}{\ln(R_{inj}/R_0^*)}} = \sqrt{1 + \frac{\ln(R_{inj}/R_{rm})}{\ln(R_0^*/R_{inj})}}, \quad (88)$$

where  $R_0^*$  is the radius of the object with mass  $m_0^*$  defined in §5.1. Assuming for illustration that on “average”  $\mu \approx 1.1$  and that at the high mass end the largest fragments produced in collisions have mass equal to 0.3 of the target mass ( $m_{0,B}(m_{inj}) = 0.3m_{inj}$ ) one finds  $\ln(R_0^*/R_{inj}) = \ln(m_{0,B}(m_{inj})/m_{inj})/3(\mu - 1) \approx 4$  and  $\delta \approx 2 - 3$ . Thus, in this particular exercise the neglect of non-power law effects leads to an *underestimate* of the mass in large bodies by a factor of several. This also implies that the total disk mass, which is dominated by the mass in large bodies, is underestimated.

An underestimate of the disk mass also leads to an underestimate of the disk lifetime,  $M_{disk}/\dot{M}_{disk}$ . This occurs because if the disk is in steady-state, then  $F(m)$  is independent of  $m$ , which means it is possible to infer  $\dot{M}_{disk}$  from infrared observations alone, without extrapolation to large masses (Wyatt, 2008). Supposing that we had correctly inferred  $\dot{M}_{disk}$  from observations, but had failed to apply the non-power law correction, and hence underestimated the disk mass, then we would also have underestimated the disk lifetime.

Based on the above discussion, breaking the assumption  $m_{0,B} \propto m_t$  affects the calculation of disk properties from observations. Conversely, observations of disks can be used to constrain the model parameters (i.e.  $\mu$  and  $C$  if  $m_{0,B}$  is given by Eq. (37)), if e.g. the inferred disk mass is found to be unreasonable for some parameter range. However, as mentioned in §6.2, direct application of our theoretical results to the observed mass spectrum of objects is complicated by the multitude of additional factors playing an important role in real astrophysical systems. Nevertheless, modern calculations (de Elía & Brunini, 2007; O’Brien & Greenberg, 2005) of the collisional evolution in the asteroid belt and of debris disks (Thébault & Augereau, 2007; Krivov et al., 2008) aim for a precision of tens of percent or less over a broad range of masses. At this level of accuracy, the non-power law effects considered in this work would play a significant role and should be taken into account.

## 7. Summary

We have shown that unless  $m_{0,B}(m_t) \propto m_t$ , where  $m_{0,B}$  is the mass of the largest fragment produced in a collision with just enough energy to disperse half of the target’s mass,  $m_t$ , to infinity, a steady-state power law solution for the mass distribution,  $n(m)$ , is not possible. The non-power law behavior is weak, however, and the solution for  $n(m)$  becomes the product of a power law and

a much more slowly varying function of the mass:  $n(m) = m^{-\alpha}\varphi(m)$ ,  $|d\ln\varphi/d\ln m| \ll 1$ . This slowly varying function is equal to a constant when  $m_{0,B}(m_t) \propto m_t$ , and the fact that previous researchers (Kobayashi & Tanaka, 2010; Tanaka et al., 1996; Dohnanyi, 1969; Petit & Farinella, 1993; O’Brien & Greenberg, 2003, 2005; Williams & Wetherill, 1994; de Elía & Brunini, 2007) have assumed just such a dependence of  $m_{0,B}(m_t)$ , explains why this kind of non-power law behavior was not observed earlier.

When  $m_{0,B}(m_t)$  is not proportional to  $m_t$ ,  $n(m)$  deviates smoothly away from a pure power law, with the deviation only becoming significant when considering many orders of magnitude in mass. This is quite different from the wavy non-power law behavior resulting from either a lower cutoff to the mass distribution due to the ejection of small particles by radiation pressure (Thébault & Augereau, 2007; Campo Bagatin et al., 1994; Durda & Dermott, 1997), a transition from a collisionally-evolved to a primordial size distribution (Fraser, 2009; Pan & Sari, 2005; Kenyon & Bromley, 2004), or a break in the power law index of the strength law (O’Brien & Greenberg, 2003, 2005). The non-power law behavior we describe in this work is significant when extrapolating over many orders of magnitude in mass, such as when inferring the number of large bodies in a system based on infrared observations (Wyatt, 2008). For instance, assuming  $m_{0,B}(m_t) \propto m_t^{1.1}$ , a deviation of only 10% in the power law index from the usual assumption of  $m_{0,B}(m_t) \propto m_t$  results in a factor of  $\sim 2 - 3$  correction when inferring the number of 10 km bodies from observations of dust.

We have quantified precisely the effect of the non-power law behavior on the mass distribution by obtaining analytical solutions for  $\varphi(m)$  in the case of a power law fragment mass distribution with  $m_B(m_t) = m_t$ , and a monodisperse fragment mass distribution (all fragments the same size) with  $m_B(m_t) = Bm_t^\beta$ . We have also provided a general framework for solving the  $m_B(m_t) = Bm_t^\beta$  case with an arbitrary fragment mass distribution. In all cases considered, our analytical solutions were confirmed numerically, and we noticed that the simple expression (84) captures the essence of the non-power law behavior for a wide range of parameters in our model.

In the course of our investigation, we have also found an entirely different type of non-power law behavior. Namely, we have discovered that fragmentation cascades can support wavy, steady-state solutions, even when there is no upper or lower mass cutoff, and the strength law is given by a pure power law. Our results were derived for the monodisperse case, but such waves may also be able to persist for more realistic fragment mass distributions. In astrophysical systems, these kinds of waves could be triggered in stochastic collisions between large planetesimals that generate enough collisional debris to significantly alter  $n(m)$ .

We are grateful to Jeremy Goodman for useful discussions. The financial support for this work is provided by the Sloan Foundation and NASA via grant NNX08AH87G.

## REFERENCES

- Benz, W., Asphaug, E., & Ryan, E. V. 1994. Numerical simulations of catastrophic disruption: Recent results. *Planet. Space Sci.* 42, 1053-1066.
- Benz, W., & Asphaug, E. 1999. Catastrophic Disruptions Revisited. *Icarus* 142, 5-20.
- Bottke, W. F., Durda, D. D., Nesvorný, D., Jedicke, R., Morbidelli, A., Vokrouhlický, D., & Levison, H. F. 2005. Linking the collisional history of the main asteroid belt to its dynamical excitation and depletion. *Icarus* 179, 63-94.
- Campo Bagatin, A., Cellino, A., Davis, D. R., Farinella, P., & Paolicchi, P., 1994. Wavy size distributions for collisional systems with a small-size cutoff. *Planet. Space Sci.* 42, 1079-1092.
- Davis, D. R., & Farinella, P. 1997. Collisional evolution of Edgeworth-Kuiper Belt objects. *Icarus* 125, 50-60.
- Davis, D. R. & Ryan, E. V. 1990. On collisional disruption - Experimental results and scaling laws. *Icarus* 83, 156-182.
- de Elía, J. C. & Brunini, A. 2007. Collisional and dynamical evolution of the main belt and NEA population. *A&A* 466, 1159-1177.
- Dohnanyi, J. S. 1969. Collisional Model of Asteroids and Their Debris. *J. Geophys. Res.* 74, 2531-2554.
- Durda, D. D. & Dermott, S. F. 1997. The collisional evolution of the asteroid belt and its contribution to the Zodiacal Cloud. *Icarus* 130, 140-164.
- Fraser, W. C. 2009. The collisional divot in the Kuiper Belt size distribution. *ApJ* 706, 119-129.
- Fujiwara, A., Kamimoto, G., & Tsukamoto, A. 1977. Destruction of basaltic bodies by high-velocity impact. *Icarus* 31, 277-288.
- Gault, D. E. & Wedekind, J. A. 1969. The destruction of tektites by micrometeoroid impact. *J. Geophys. Res.* 74, 6780-6794.
- Greenberg, R. & Nolan, M. C. 1989. Delivery of asteroids and meteorites to the inner Solar System. In: R. P. Binzel, T. Gehrels and M. S. Matthews, Editors, *Asteroids II*, Univ. of Arizona Press, Tucson (1989), pp. 778-804.
- Holsapple, K. A. 1993. The scaling of impact processes in planetary sciences. *Ann. Rev. Earth Planet. Sci.* 21, 333-373.
- Housen, K. R., Schmidt, R. M., & Holsapple, K. A. 1991. Laboratory simulations of large scale fragmentation events. *Icarus* 94, 180-190.

- Kennedy, G. M., & Wyatt, M. C. 2011. Collisional evolution of irregular satellite swarms: detectable dust around Solar system and extrasolar planets. *MNRAS* 135.
- Kenyon, S. J., & Bromley, B. C. 2004. The size distribution of Kuiper Belt objects. *AJ* 128, 1916-1926.
- Kenyon, S. J., & Bromley, B. C. 2005. Prospects for detection of catastrophic collisions in debris disks. *AJ* 130, 269-279.
- Kenyon, S. J., & Bromley, B. C. 2010. Variations on Debris Disks. II. Icy Planet Formation as a Function of the Bulk Properties and Initial Sizes of Planetesimals. *ApJS* 188, 242-279.
- Kobayashi, H., & Tanaka, H. 2010. Fragmentation model dependence of collision cascades. *Icarus* 206, 735-746.
- Krivov, A. V., Müller, S., Löhne, T., & Mutschke, H. 2008. Collisional and thermal emission models of debris disks: toward planetesimal properties. *ApJ* 687, 608-622.
- O’Brien, D. P., & Greenberg, R. 2003. Steady-state size distributions for collisional populations: analytical solution with size-dependent strength. *Icarus* 164, 334-345.
- O’Brien, D. P., & Greenberg, R. 2005. The collisional and dynamical evolution of the main-belt and NEA size distributions. *Icarus* 178, 179-212.
- Pan, M., & Sari, R. 2005. Shaping the Kuiper belt size distribution by shattering large but strengthless bodies. *Icarus* 173, 342-348.
- Petit, J.-M., & Farinella, P. 1993. Modelling the outcomes of high-velocity impacts between small solar system bodies. *Celestial Mechanics and Dynamical Astronomy* 57, 1-28.
- Polyanin, A.D., & Manzhirov, A.V. “Handbook of integral equations: exact solutions (Supplement. Some functional equations)”, [in Russian]; Faktorial, Moscow, 1998.
- Stewart, S. T., & Leinhardt, Z. M. 2009. Velocity-dependent catastrophic disruption criteria for planetesimals. *ApJ* 691, L133-L137.
- Takagi, Y., Muzitani, H., & Kawakami, S. 1984. Impact fragmentation experiments of basalts and pyrophyllites. *Icarus* 59, 462-477.
- Tanaka, H., Inaba, S., & Nakazawa, K. 1996. Steady-state size distribution for the self-similar collision cascade. *Icarus* 123, 450-455.
- Thébault, P., & Augereau, J.-C. 2007. Collisional processes and size distribution in spatially extended debris disks. *A&A* 472, 169-185.
- Williams, D. R. & Wetherill, G. W. 1994. Size distribution of collisionally evolved asteroidal populations - Analytical solution for self-similar collision cascades. *Icarus* 107, 117-128.

Wyatt, M. C. 2008. Evolution of debris disks. *ARA&A* 46, 339-383.

Wyatt, M. C., & Dent, W. R. F. 2002. Collisional processes in extrasolar planetesimal disks. *MNRAS* 334, 589-607.

### A. Convergence of the Mass Flux Integral

We discuss here the convergence of the mass flux integrals in §3.1,3.2. If the correct value of  $\alpha$  is substituted into Eq. (42) or Eq. (43), then the mass flux takes the form

$$F(m) \propto \int_0^1 dx x^{-1} \int_0^\infty dy y^{-\alpha} f(x, y). \quad (\text{A1})$$

It is helpful to discuss under what circumstances the integrals in this expression converge.

The integral over  $y$  converges at its upper limit if  $\alpha > 1$ , because  $f(x, y) < 1$ . There is actually already a more stringent condition of  $\alpha > 5/3$ , which comes from the requirement that the cross-section be dominated by the smallest particles (§2.1), so the requirement  $\alpha > 1$  is automatically fulfilled.

We now consider convergence of the integral over  $y$  at its lower limit. Generally speaking, the quantity  $f(x, y)y^{-\alpha}$  drops off for  $y \ll 1$ , the threshold for catastrophic breaking, which leads to convergence. In fact, in a model without erosion,  $f(x, y) = 0$  for  $y < 1$ , so there is a sharp cutoff at  $y = 1$ . In reality, erosion will smooth this cutoff, but as long as  $f(x, y)$  falls off faster than  $y^{\alpha-1}$  for  $y \ll 1$ , then the integral will converge at its lower limit. We point out that if the integral over  $y$  converges, then it follows from the above arguments that  $f(x, y)y^{-\alpha}$  is peaked at  $y_{peak} = k$ . In the absence of erosion, it is clear that  $k \sim 1$ , but when erosion is considered, we typically have  $k \ll 1$  (Kobayashi & Tanaka, 2010).

We next consider the convergence of the integral over  $x$ , and we find it helpful to define

$$f(x) \equiv \int_0^\infty dy y^{-\alpha} f(x, y) \quad (\text{A2})$$

As long as  $f(x)$  is bounded on  $x \in [0, 1]$ , then the integral over  $x$  in Eq. (A1) converges at the upper limit of integration. At the lower limit of integration, the function  $x^{-1}$  diverges, but only logarithmically, so if  $f(x) \rightarrow 0$  for  $x \ll 1$ , then we would typically expect convergence at the lower limit. From Eq. (7) and Eq. (22), we have  $f(x, y) \rightarrow 0$  for  $x \ll 1$ , so we do indeed expect  $f(x) \rightarrow 0$  in the same limit.

## B. Details of the calculation of $\varphi(m)$ .

We start by developing a general method for calculating  $\varphi(m)$  for different forms of  $m_B(m)$  from the functional Eq. (57) with known  $\Theta(m)$ .

### B.1. Case $m_B(m) = Bm$ , $\beta = 1$

Here, we will first assume following Dohnanyi (1969) and Tanaka et al. (1996) that  $m_B(m) = Bm$ . Then, we need to solve the functional equation

$$\varphi(m)\varphi(Bm) = \Theta(m). \quad (\text{B1})$$

Taking the logarithm of both sides of this equation we get

$$\ln \varphi(m) + \ln \varphi(Bm) = \ln \Theta(m), \quad (\text{B2})$$

and upon introducing the new independent variable  $v \equiv \ln m$ , the constant  $b \equiv \ln B$ , and the new function  $\varphi_1(s) \equiv \ln \varphi(e^s)$  one gets

$$\varphi_1(v) + \varphi_1(v + b) = R_1(v), \quad R_1(v) \equiv \ln \Theta(e^v). \quad (\text{B3})$$

For some applications, it is more appropriate to study an equivalent equation

$$\varphi_1(u - b) + \varphi_1(u) = R_1(u - b). \quad (\text{B4})$$

One can check by direct substitution that the formal solution of Eq. (B3) up to an additive constant  $\varphi_1(-\infty)$  is given by

$$\varphi_1(v) + \varphi_1(-\infty) = \sum_{k=0}^{\infty} (-1)^k R_2(v + kb), \quad (\text{B5})$$

where we have used the fact that  $b < 0$ , since  $B < 1$ . It follows then, that  $\varphi$  is given up to an overall normalization constant  $\varphi(0)$  as

$$\frac{\varphi(m)}{\varphi(0)} = \exp \left[ \sum_{k=0}^{\infty} (-1)^k \ln \Theta(e^{\ln m + kb}) \right] = \prod_{k=0}^{\infty} \frac{\Theta(me^{2kb})}{\Theta(me^{(2k+1)b})}. \quad (\text{B6})$$

Analogously, the solution of Eq. (B4) up to an additive constant and the corresponding solution for  $\varphi$  up to a normalization are given by

$$\varphi_1(v) + \varphi_1(\infty) = \sum_{k=0}^{\infty} (-1)^k R_1(v - (k+1)b), \quad (\text{B7})$$

$$\frac{\varphi(m)}{\varphi(\infty)} = \prod_{k=0}^{\infty} \frac{\Theta(me^{-(2k+1)b})}{\Theta(me^{-(2k+2)b})}. \quad (\text{B8})$$

In §B.3.1 we provide an example of how to discriminate between using Eq. (B6) versus Eq. (B8) to calculate  $\varphi$ .



## B.2. Case $m_B(m) = Bm^\beta$ , $\beta \neq 1$

Whenever  $\beta \neq 1$  we need to solve the functional Eq.  $\varphi(m)\varphi(Bm^\beta) = \Theta(m)$ , which is easily converted to

$$\ln \varphi(m) + \ln \varphi(Bm^\beta) = \ln \Theta(m). \quad (\text{B9})$$

Invoking the mass scale  $m_B^* \equiv B^{1/(1-\beta)}$  at which breaking stops (i.e.  $m_B(m_B^*) = m_B^*$ ), and defining the new independent variable  $u \equiv \ln |\ln(m/m_B^*)|$ ,  $-\infty < u < \infty$  and the new function  $\varphi_2(s) \equiv \ln \varphi(m_B^* e^{e^s})$  one obtains

$$\varphi_2(u) + \varphi_2(u + a) = R_2(u), \quad R_2(u) \equiv \ln \Theta(m_B^* e^{e^u}), \quad a \equiv \ln \beta. \quad (\text{B10})$$

This equation can also be converted to an equivalent form useful in some applications:

$$\varphi_2(u - a) + \varphi_2(u) = R_2(u - a). \quad (\text{B11})$$

Analogous to the previous case, we can write down formal solutions of Eq. (B10) and Eq. (B11) up to additive constants, and the corresponding solutions for  $\varphi$  up to normalization constants. For  $\beta > 1$ , we have  $a > 0$ , which yields for Eq. (B10)

$$\varphi_2(u) + \varphi_2(\infty) = \sum_{k=0}^{\infty} (-1)^k R_2(u + ka), \quad (\text{B12})$$

$$\frac{\varphi(m)}{\varphi(0)} = \prod_{k=0}^{\infty} \frac{\Theta(m_B^* \exp(e^{2ka} \ln \frac{m}{m_B^*}))}{\Theta(m_B^* \exp(e^{(2k+1)a} \ln \frac{m}{m_B^*}))}, \quad (\text{B13})$$

and for Eq. (B11)

$$\varphi_2(u) + \varphi_2(-\infty) = \sum_{k=0}^{\infty} (-1)^k R_2(u - (k+1)a), \quad (\text{B14})$$

$$\frac{\varphi(m)}{\varphi(m_B^*)} = \prod_{k=0}^{\infty} \frac{\Theta(m_B^* \exp(e^{-(2k+1)a} \ln \frac{m}{m_B^*}))}{\Theta(m_B^* \exp(e^{-(2k+2)a} \ln \frac{m}{m_B^*}))}. \quad (\text{B15})$$

In a similar fashion, we can obtain the solutions when  $\beta < 1$ , in which case  $a < 0$ . We have for Eq. (B10)

$$\varphi_2(u) + \varphi_2(-\infty) = \sum_{k=0}^{\infty} (-1)^k R_2(u + ka), \quad (\text{B16})$$

$$\frac{\varphi(m)}{\varphi(m_B^*)} = \prod_{k=0}^{\infty} \frac{\Theta(m_B^* \exp(e^{2ka} \ln \frac{m}{m_B^*}))}{\Theta(m_B^* \exp(e^{(2k+1)a} \ln \frac{m}{m_B^*}))}, \quad (\text{B17})$$

and for Eq. (B11)

$$\varphi_2(u) + \varphi_2(\infty) = \sum_{k=0}^{\infty} (-1)^k R_2(u - (k+1)a), \quad (\text{B18})$$

$$\frac{\varphi(m)}{\varphi(\infty)} = \prod_{k=0}^{\infty} \frac{\Theta\left(m_B^* \exp\left(e^{-(2k+1)a} \ln \frac{m}{m_B^*}\right)\right)}{\Theta\left(m_B^* \exp\left(e^{(-2k+2)a} \ln \frac{m}{m_B^*}\right)\right)}. \quad (\text{B19})$$

This completes the description of the general mathematical formalism needed for finding  $\varphi(m)$  given  $\Theta(m)$  and given  $m_B(m)$  in power law form. We now obtain explicit expressions for  $\varphi(m)$  for a monodisperse fragment mass distribution.

### B.3. Application to the monodisperse case

#### B.3.1. Case $m_B(m) = Bm^\beta$ , $\beta = 1$

In the monodisperse case, we can take

$$\Theta(m) = \frac{1}{\ln(m/m_{0,B}(m))} = \frac{1}{(1-\mu) \ln m - \ln C}, \quad (\text{B20})$$

where we will again assume  $m_{0,B}(m) = Cm^\mu$ . Considering the case  $\beta = 1$ , the two relevant equations for obtaining  $\varphi(m)$  are Eq. (B6) and Eq. (B8). The  $\varphi(0)$  term in the denominator on the left hand side of Eq. (B6) means that this equation is only applicable when  $\mu > 1$ , since for  $\mu < 1$  there is a value  $m_0^*$  below which  $m_{0,B}(m) > m$ , and the solution is unphysical below this point. Similarly, the  $\varphi(\infty)$  term in the denominator on the left hand side of Eq. (B8) means that the solution only works for  $\mu < 1$ , because for  $\mu > 1$ ,  $m_{0,B}(m) > m$  above  $m_0^*$ , and the solution is again unphysical.

Treating first the  $\mu > 1$  case, if we substitute Eq. (B20) into Eq. (B6), we have

$$\frac{\varphi(m)}{\varphi(0)} = \prod_{k=0}^{\infty} \frac{\ln\left(\frac{m}{m_{0,B}(m)}\right) + (2k+1)(1-\mu)b}{\ln\left(\frac{m}{m_{0,B}(m)}\right) + 2k(1-\mu)b}. \quad (\text{B21})$$

Unfortunately, this expression does not converge, implying that  $\varphi(0) = 0$ . To understand this behavior, we can refer back to the analytic solution for  $\varphi$  in the monodisperse case with  $m_B(m) = m$  (Eq. (84)). There, we had  $\varphi(m) = 1/\sqrt{\ln(m/m_{0,B}(m))}$ . For  $\mu > 1$ , this expression does indeed yield  $\varphi(0) = 0$ .

Since  $\varphi(m)$  is only defined up to a normalization, we can remedy the situation by working with the *ratio* of  $\varphi(m)$  at two points rather than with  $\varphi(m)$  itself, which gives a convergent expression.

If we define  $a_1 \equiv \ln(m_1/m_{0,B}(m_1))$ ,  $a_2 \equiv \ln(m_2/m_{0,B}(m_2))$ , and  $c \equiv (1 - \mu)b$ , then it follows from expression (B21) that

$$\frac{\varphi(m_1)}{\varphi(m_2)} = \prod_{k=0}^{\infty} \frac{(a_1 + (2k+1)b)(a_2 + 2kb)}{(a_1 + 2kb)(a_2 + (2k+1)b)}, \quad (\text{B22})$$

which simplifies to

$$\frac{\varphi(m_1)}{\varphi(m_2)} = \frac{a_2 \Gamma\left(1 + \frac{a_1}{2c}\right) \Gamma\left(\frac{1}{2} + \frac{a_2}{2c}\right)}{a_1 \Gamma\left(1 + \frac{a_2}{2c}\right) \Gamma\left(\frac{1}{2} + \frac{a_1}{2c}\right)}. \quad (\text{B23})$$

The correctness of this solution can be verified directly by substituting  $\varphi$  back into Eq. (57), and using (B20) for  $\Theta(m)$ .

Treating next the  $\mu < 1$  case, if we substitute Eq. (B20) into Eq. (B8), we have

$$\frac{\varphi(m)}{\varphi(\infty)} = \prod_{k=0}^{\infty} \frac{\ln\left(\frac{m}{m_{0,B}(m)}\right) - (2k+2)(1-\mu)b}{\ln\left(\frac{m}{m_{0,B}(m)}\right) - (2k+1)(1-\mu)b}. \quad (\text{B24})$$

Again, this equation does not converge, but the ratio of  $\varphi$  at two points does, and using the same definitions for  $a_1$ ,  $a_2$ , and  $c$  as before, we have

$$\frac{\varphi(m_1)}{\varphi(m_2)} = \frac{\Gamma\left(1 - \frac{a_2}{2c}\right) \Gamma\left(\frac{1}{2} - \frac{a_1}{2c}\right)}{\Gamma\left(1 - \frac{a_1}{2c}\right) \Gamma\left(\frac{1}{2} - \frac{a_2}{2c}\right)}. \quad (\text{B25})$$

### B.3.2. Case $m_B(m) = Bm^\beta$ , $\beta \neq 1$

We now treat the case when the mass of the smallest projectile that can catastrophically shatter a target is not proportional to the mass of the target itself, so that  $\beta \neq 1$ .

We first consider the case  $\beta > 1$ , so we have the choice of using Eq. (B13) or Eq. (B15), and we limit ourselves to the situation when  $m_{0,B}(m_B^*) < m_B^*$ . We expect such a situation to be realistic, since the maximum fragments created by the disruption of bodies with mass close to  $m_B^*$ , should still be smaller than  $m_B^*$ . Without this assumption,  $\varphi(m_B^*)$  would be unphysical, since we would have  $m_{0,B}(m_B^*) > m_B^*$ , which is impossible in a fragmentation cascade. Given this assumption, we can use Eq. (B15) to solve for  $\varphi$  up to a normalization.

Substituting Eq. (B20) into Eq. (B15), we have

$$\frac{\varphi(m)}{\varphi(m_B^*)} = \prod_{k=0}^{\infty} \frac{\ln\left(\frac{m}{Dm_{0,B}(m)}\right) \beta^{-(2k+2)} + \ln D}{\ln\left(\frac{m}{Dm_{0,B}(m)}\right) \beta^{-(2k+1)} + \ln D}, \quad (\text{B26})$$

where we have defined the constant  $D \equiv C^{-1} B^{(1-\mu)/(1-\beta)} = (m_B^*/m_0^*)^{1-\mu}$ . In this case, the product does converge since  $\varphi(m_B^*)$  is nonzero (it is also finite), and we do not have to take the ratio of two points as we did for the  $\beta = 0$  case in §B.3.1.

Next, we consider the case  $\beta < 1$ , and now we have the choice of using Eq. (B17) or Eq. (B19). We again make the assumption that  $m_{0,B}(m_B^*) < m_B^*$ , in which case we can use Eq. (B17) to obtain

$$\frac{\varphi(m)}{\varphi(m_B^*)} = \prod_{k=0}^{\infty} \frac{\ln\left(\frac{m}{Dm_{0,B}(m)}\right) \beta^{2k+1} + \ln D}{\ln\left(\frac{m}{Dm_{0,B}(m)}\right) \beta^{2k} + \ln D}. \quad (\text{B27})$$

Again, there are no problems with convergence. Note, that if we set  $\mu = 1$  then  $m/m_{0,B}(m) = \text{const}$  and Eq. (B26) and Eq. (B27) yield  $\varphi(m) = \text{const}$  in agreement with O’Brien & Greenberg (2003).

### C. Fragmentation Code

We describe here the numerical algorithm we use to study fragmentation. We differ from the main text here in that our algorithm evolves the differential number density of particles  $n(r)$  per unit radius, rather than particle mass, but it is straightforward to convert between  $n(m)$  and  $n(r)$ .

The evolution equation for  $n(r)$  can be written as the sum of a source term (denoted by a plus sign) and a sink term (denoted by a minus sign):

$$\frac{\partial n}{\partial t}(r, t) = \frac{\partial n_-}{\partial t}(r, t) + \frac{\partial n_+}{\partial t}(r, t). \quad (\text{C1})$$

The sink term is simply given by the number of catastrophic collisions that particles with radius  $r$  are undergoing per unit time. Dropping the dependence on time for brevity (everything is evaluated at time  $t$ ) and ignoring erosion, we can write

$$\frac{\partial n_-}{\partial t}(r) = -\pi v n(r) \int_{r_B(r)}^{\tilde{r}_B(r)} dr' n(r') (r + r')^2, \quad (\text{C2})$$

where  $r_B(r)$  is the minimum particle size that can fragment a particle of radius  $r$ ,  $\tilde{r}_B(r)$  is defined analogously to  $\tilde{m}_B(m)$ , and we have assumed that the particle cross-section is the geometric cross-section, and that the impact velocity is a constant §2.1.

For the source term, we will first state the equation and then analyze it piece by piece:

$$\frac{\partial n_+}{\partial t}(r) = \pi v \int_r^{\infty} dr_1 n(r_1) \int_{r_B(r_1)}^{\tilde{r}_B(r_1)} dr_2 n(r_2) h(r, r_1, r_2) (r_1 + r_2)^2. \quad (\text{C3})$$

Here, we have used  $r_1$  to denote a target and  $r_2$  a projectile with the possibility that  $r_2 > r_1$ . Now,  $\pi v n(r_1) n(r_2) (r_1 + r_2)^2 dr_2 dr_1$  gives the number of collisions (per unit volume per unit time) between targets in the range  $r_1$  to  $r_1 + dr_1$  and projectiles in the range  $r_2$  to  $r_2 + dr_2$ . We define  $h(r, r_1, r_2) dr$  to be the number of fragments in the size range  $r$  to  $r + dr$  from destruction of the target particle only. Then  $h(r, r_1, r_2) n(r_1) n(r_2) \mathcal{R}(r_1, r_2) dr_2 dr_1 dr$  gives the particle flux into the range  $r$  to  $r + dr$  from targets in the range  $r_1$  to  $r_1 + dr_1$  that have been shattered by projectiles in

the range  $r_2$  to  $r_2 + dr_2$ . Then, we simply integrate this expression over all values of  $r_1 > r$  and all values of  $r_2$ , which yield a catastrophic fragmentation event (i.e. an event in which both the target and the projectile are destroyed).

A useful simplification of Eq. (C3) can be obtained if we assume that the distribution of fragments is independent of the projectile size so that  $h(r, r_1, r_2) \rightarrow h(r, r_1)$ . In this case, which is adopted for the numerical calculations in this work (§5), equation (C3) becomes

$$\frac{\partial n_+}{\partial t}(r) = \pi v \int_r^\infty dr_1 h(r, r_1) n(r_1) \int_{r_B(r_1)}^{\tilde{r}_B(r_1)} dr_2 n(r_2) (r_1 + r_2)^2, \quad (\text{C4})$$

and comparing with Eq. C2 we see that we can write

$$\frac{\partial n_+}{\partial t}(r) = - \int_r^\infty dr' h(r, r') \frac{\partial n_-}{\partial t}(r'). \quad (\text{C5})$$

This is a useful form of the source equation when it comes to computations, because it reduces a double integral to a single integral, once the sink term has been calculated.

Given a starting distribution for  $n(r)$  and a form for  $h(r, r')$  (e.g. monodisperse, power law, etc.), it is possible to evolve the distribution forward in time using discretized versions of Eq. (C2) and Eq. (C5) in  $\log r$  space. The integrals in these equations are performed using standard numerical integration techniques, such as the trapezoid or Simpson’s rule. This results in an efficient order  $O(N)$  method, where  $N$  is the number of radius bins which are equally spaced in  $\log r$ . The scaling of the method is important for us, since to resolve the non-power law behavior we use up to  $\sim 3000$  bins per decade in  $r$ , yielding a total of  $\sim 10^5$  bins.

In order to advance the distribution in time, a timestep must be specified. A good criterion is to set it to a fixed fraction of the shortest collision time in the simulation. This ensures that the particle size distribution can never become negative. Another problem is dealing with the boundaries of the simulation. The upper boundary is generally not problematic since the collision time there is long compared to the rest of the simulation, and the maximum particle size can be chosen to be as large as necessary for there to be negligible variation in the particle mass distribution at the high mass end. The lower boundary, however, can be a problem if  $r_B(r) \ll r$  there. In this case, extrapolation of the particle mass distribution to lower masses is necessary, and care must be taken to ensure that the simulation is stable.